**An N-glycan on the C2 domain of JAGGED1 is important for Notch activation**

Yao Meng [1,9], Sami Sanlidag[2,3], Sacha A. Jensen[1,4], Sean A. Burnap[5], Weston B. Struwe[5], Andreas H. Larsen[1,6], Xinyi Feng[1], Shruti Mittal[1], Mark S.P. Sansom[1], Cecilia Sahlgren[2,3,7,8] and Penny A. Handford[1*]

[1] Department of Biochemistry, University of Oxford, UK OX1 3QU

[2] Faculty for Science and Engineering, Biosciences, Åbo Akademi University, Turku, Finland

[3] Turku Bioscience Centre, Åbo Akademi University and University of Turku, Turku, Finland

[4] Current address: College of Public Health, Medical and Veterinary Sciences, James Cook University, Townsville, Queensland, Australia

[5] Kavli Institute for NanoScience Discovery and Physical and Theoretical Chemistry Laboratory, Department of Chemistry, University of Oxford, Oxford, UK

[6] Current address: Department of Neuroscience, University of Copenhagen, Copenhagen, Denmark

[7] Department of Biomedical Engineering, Eindhoven University of Technology, Eindhoven, The Netherlands

[8] Institute for Complex Molecular Systems, Eindhoven University of Technology, Eindhoven, The Netherlands

[9] Current address: Institute of Medicinal Biotechnology, Chinese Academy of Medical Sciences and Peking Union Medical College, Beijing, China

*Corresponding author. Email: penny.handford@bioch.ox.ac.uk

**Abstract**

The canonical members of the Jagged/Serrate and Delta families of transmembrane ligands have an extracellular, N-terminal C2 domain that binds to phospholipids and is required for optimal activation of the Notch receptor. Somatic mutations that cause amino substitutions in the C2 domain in human JAGGED1 (JAG1) have been identified in tumors. We found in reporter cell assays that mutations affecting an N-glycosylation site reduced the ligand's ability to activate Notch. This N-glycosylation site located in the C2 domain is conserved in the Jagged/Serrate family but lacking in the Delta family. Site-specific glycan analysis of the JAG1 N-terminus demonstrated that occupancy of this site by either a complex-type or high mannose N-glycan was required for full Notch activation in reporter cell assays. Similarly to JAG1 variants with defects in Notch binding, N-glycan removal, either by mutagenesis of the glycosylation site or by endoglycosidase treatment, reduced receptor activation. The N-glycan variants also reduced receptor activation in a Notch signaling–dependent vascular smooth muscle cell differentiation assay. Loss of the C2 N-glycan reduced JAG1 binding to liposomes to a similar extent as the loss of the entire C2 domain. Molecular dynamics simulations suggested that the presence of the N-glycan limits the orientation of JAG1 relative to the membrane, thus facilitating Notch binding. These data are consistent with a critical role for the N-glycan in promoting a lipid-binding conformation that is required to orient Jagged at the cell membrane for full Notch activation.

## Introduction

The Notch pathway is a key signal transduction pathway in metazoans, crucial for many cell fate decisions during development and homeostasis (*1*). As a consequence, pathway dysregulation contributes to many inherited and acquired diseases, including cerebral autosomal dominant arteriopathy with subcortical infarcts and leukoencephalopathy (CADASIL), Alagille syndrome, and various cancers (*2*, *3*). Canonical Notch signaling requires receptor and ligand components, both of which are single-pass transmembrane proteins, present on opposing cell surfaces. Binding of the receptor, Notch, by ligands of the Jagged and Serrate (Jagged/Serrate) or Delta families, followed by ligand endocytosis, results in removal of the ligand-bound Notch extracellular domain through cleavage within the negative regulatory region (NRR) and exposes the remaining membrane-anchored Notch moiety to further proteolytic cleavage (*4*). The final intra-membrane cleavage releases the intracellular domain of Notch, which translocates to the nucleus and, in combination with the putative transcriptional coactivator Mastermind-like, binds to a transcription factor of the CBF1, Suppressor of Hairless, Lag-1 (CSL) family to relieve repression of targets genes, such as those of the *Hes* and *Hey* families (*5*, *6*).

Structural work has yielded fundamental insights into the extracellular receptor-ligand complex. The structure of the isolated N-terminus of human Jagged1 (JAG1) revealed the presence of a $Ca2^{+}$-dependent, phospholipid-binding C2 domain that is important for Notch activation (*7*). High-resolution structures of the corresponding regions from human ligands JAG2 and Delta-like4 (DLL4) and a larger fragment of DLL1 all confirm the presence of this domain, with the ligand families distinguished by the presence of $Ca^{2+}$ binding sites in Jagged, but not in Delta,

ligands (*8*, *9*). Notable are the differences in the β1-2, β5-6 apical loop regions, shown by crystallography to mediate lipid binding by certain intracellular proteins containing C2 domains such as cytosolic phospholipase A2α, suggesting the occurrence of ligand-specific membrane interactions (*10*). Interplay is observed between Notch and lipid binding to ligand in functional assays, suggesting that all are needed to form a ternary complex for optimal Notch activation (*8*). Structures of rat Dll4 in complex with the epidermal growth factor–like (EGF) domains 11-13 of Notch and of rat Jag1 in complex with Notch EGF domains 8-12 show that the Notch EGF11-12 ligand-binding region (LBR) is in an antiparallel orientation with respect to each ligand, and two core sites of interaction (site 1 C2-EGF12, site 2 Delta Serrate Lag2 (DSL)-EGF11) are present (*11*, *12*). Different O-glycan requirements for the formation of each ligand-receptor complex are observed, thus providing molecular insight into the known role of O-glycosylation in regulating Notch activity (*13*). In conjunction with many functional studies, these data implicate mechanical force, O-glycans, and lipid binding in tuning the Notch signal and emphasize the important role of the C2 domain in organizing the receptor-ligand complex at the membrane (*13–15*).

Although membrane interactions mediated by the N-terminal C2 domain are clearly involved in the Notch activation process, mechanistic insight is lacking. A small subset of disease-causing variants associated with extra-hepatic biliary atresia (EHBA) with substitutions in the JAG1 C2 β1-2 apical phospholipid-binding loop are defective in their ability to activate Notch, as is the engineered variant D140A-D144A, which was designed to reduce $Ca^{2+}$ binding to the apical loop region (*8*). An in vivo *Drosophila melanogaster* study has demonstrated that a deletion of 5 amino acids in the β1-2 loop of the Delta ligand produces Notch signaling defects in the wing, sensory bristles (microchaete), and photoreceptors, further emphasizing that this loop is required

for optimal ligand function (*16*).

To further investigate the function of the mammalian C2 domain, we constructed a series of JAG1 variants with amino acid substitutions affecting the loop regions as well as the hydrophobic core. These variants were identified from missense mutations reported in the Catalogue of somatic mutations in cancer (COSMIC) database (*17*). Many of the variants we investigated caused loss of function, but amongst the most deleterious was one that altered an N-glycosylation sequence in the β5-6 apical phospholipid-binding loop. An N-glycan has been observed in this position in some ligand crystal structures, but not others, depending upon the method used for protein expression, purification, and crystallization (*7*, *8*, *12*). The N-glycosylation sequon NxS/T on the β5-6 loop was 100% conserved in Jagged ligands but absent from all Delta ligands in higher metazoans. Mutating the N-glycosylation site in an N-terminal fragment of wild-type (WT) JAG1, producing protein in N-glycosylation–defective cells, or enzymatic removal of the sugar from this fragment led to poor Notch activation and impaired liposome binding. Through glycoproteomic analysis, we identified a complex-type N-glycan that, when modelled onto previously identified ligand-N-glycan structures, localised to a specific face of the JAG1 C2 domain. Molecular dynamics studies suggested that the N-glycan, together with adjacent ligand domains, restricts the number of possible interactions of the C2 domain with the membrane. Collectively, these data identify a critical functional role for the C2 N-glycan in promoting a JAG1-specific orientation at the membrane that is essential for Notch activation, and extend our knowledge of the repertoire of lipid recognition in cell signaling by C2 domains.

**Results**

**Cancer-associated JAG1 C2 variants show loss-of-function phenotypes**

We expressed twelve recombinant JAG1 variants with C2 domain substitutions (F35L, G47R, A58V, D72N, V86F, G89E, G114D, T133R, L135F, W139S, S142N, and T145N) and the DSL domain substitution E228K, all of which were identified in the COSMIC database, as fusion proteins in HEK293T cells. Each construct was expressed as a soluble extracellular fragment comprising the N-terminal C2 domain, DSL domain, and EGF domains 1-3 with both His and Fc tags at the C-terminus (fig.S1). The corresponding WT construct (J1-WT) was previously shown to be sufficient for Notch activation in a split luciferase reporter cell line (*8*) and showed similar activity to an Fc-tagged protein comprising the entire extracellular domain (J1-FL, fig. S1 and S6B). Four of the variants (F35L, G47R, T133R, and W139S) affected folding of the hydrophobic core and were not secreted, but the others were efficiently secreted into the extracellular medium and purified to near homogeneity (>90 % by reducing/non-reducing SDS-PAGE) by immobilized metal affinity chromatography (IMAC) and size exclusion chromatography (SEC) for subsequent use in Notch activation assays (fig. S2, A to C). Purified variants were tested for their ability to activate Notch and compared to J1-WT and negative control proteins F207A, F207A/E228K, which are defective in Notch binding (*18*). Many showed a reduced ability to activate Notch (fig. S3, A to D).

**An N-glycosylation site within the Jagged1 β5-6 loop is important for Notch reporter activation**

Among the secreted COSMIC variants tested, T145N altered the N-glycosylation sequence NxT on the JAG1 C2 domain β5-6 apical loop. Because this variant was associated with very low

amounts of Notch activation compared to the effect of S142N on the same loop (fig. S3, A to D), it suggested a previously unrecognised role for the N-glycan. Sequence analysis showed conservation of the NxT/S motif on the β5-6 loop in the Jagged, but not Delta, ligand families, with the exception of the *Drosophila* ligands Serrate and Delta, both of which contain the motif (Fig. 1, A). Modeling showed that the β5-6 loop of JAG1 could accommodate an N-glycan (Fig. 1B). To further investigate function, we engineered an N143A substitution in the C2 domain of JAG1 and compared it to a similar change (N217A) to a nonconserved N-glycosylation sequence in the DSL domain. SDS-PAGE analysis of purified N-glycan variants N143A, N217A, and T145N demonstrated a mass reduction compared to J1-WT that is consistent with loss of an N-glycan in either the C2 or DSL domain (Fig. 1C). Each variant's ability to activate Notch was assessed in mNotch1 and mNotch2 split luciferase reporter cell lines (HEK293T mN1-Nluc-CLuc-RBPjk and HEK293T mN2-Nluc-CLuc-RBPjk, respectively) and a yellow fluorescent protein (YFP)-based NOTCH1 reporter line (CHO hN1G4$^{esn}$) (Fig. 2, A to D). N143A showed a similar reduction as T145N in its ability to activate Notch in assay systems using either a luminescent (Fig. 2, A and B) or YFP fluorescent (Fig. 2, C and D) readout, whilst loss of the DSL N-glycan in N217A had no observable effect and activated Notch similarly to J1-WT. Both N143A and T145N substitutions on the β5-6 loop resulted in lower amounts of Notch activation than did S142N, suggesting that loss of the N-glycan was much more deleterious for function than a single amino acid substitution on the same loop. The mNotch2 reporter line was less sensitive to the effect of ligand substitutions than the mNotch1 reporter line, but N-glycan–defective variants were the least active in both of these luciferase reporter lines (Fig. 2, A and B). To exclude the possibility that the amino acid substituted within the NxS/T sequon was itself the

cause of the reduced Notch activation we observed, an N143Q variant was also also tested and found to behave similarly to the N143A and T145N variants ( fig. S4, A to C).

**N-glycan analysis**

J1-WT, expressed in HEK293T cells, was subjected to glycoproteomic analysis to identify the nature of the C2 N-glycan. Following SDS-PAGE, tryptic digestion of gel-extracted protein, and liquid chromatography–mass spectrometry (LC-MS) analysis, complex-type glycans were identified on both $Asn^{143}$ and $Asn^{217}$ residues in the C2 and DSL domains, respectively (fig. S5A). Specifically, tri- and tetra-antennary structures with varying degrees of sialylation and fucosylation were identified as the major species on glycosylated peptides containing either the β5-6 loop or DSL N-glycan sequence. Although glycoproteomics analysis suggested $Asn^{143}$ to be only 40% occupied with glycans, this is likely due to oversampling of the non-glycosylated peptides because SDS-PAGE data (Fig. 1C) demonstrated J1-WT was nearly fully glycosylated. The tetra-antennary form of the complex-type glycan on the β5-6 loop was modelled onto the known structure of JAG1, which was obtained without N-glycosylation, based on crystal structures of other N-glycan–modified ligands (Fig. 1B). The sugar occupies a large volume on one face of the ligand, away from the Notch-binding surface.

We further investigated the N-glycan requirement for activity by expressing J1-WT in HEK293S cells, which lack MGAT1, the enzyme responsible for the conversion of high mannose to hybrid and complex N-glycans. This purified J1-WT , which had oligomannose in place of complex-type glycans, activated Notch similarly to J1-WT expressed in HEK293T cells (fig. S5A to C), indicating that an oligomannose N-glycan at $Asn^{143}$ was sufficient to allow activation of Notch in reporter assays.

**Loss of β5-6 sugar attachment impairs Notch activation**

To confirm that the decrease in Notch activation by variants T145N, N143A, and N143Q was due to loss of the N-glycan on the C2 domain (rather than to partial misfolding of the domain in the absence of the sugar), we subjected J1-WT purified from HEK293T and HEK293S cells to digestion by PNGase F prior to activity assessment (*19*). PNGase F will remove both the C2 and DSL N-glycans within the ligand construct; however, because analysis of the N217A variant demonstrated that removal of the DSL glycan did not affect Notch activation in reporter lines (Fig. 2, A to C), this method can be used to assess the impact of removing the C2 N-glycan from the folded protein. A control undigested sample was subjected to incubation conditions in parallel with the PNGaseF-treated protein, and following SDS-PAGE analysis, the ability of these samples to activate Notch was tested in the CHO reporter line with a YFP readout (fig. S6A). PNGaseF-digested J1-WT showed a substantial decrease in its ability to activate Notch compared with the original starting material and the undigested control sample, whereas an equivalent DLL4 construct that has the same domain organisation as J1-WT but lacks the β5-6 N-glycan, showed normal Notch activation after digestion (fig. S6A). PNGaseF-treated J1-WT expressed in HEK293S cells (fig. S5C) or PNGase-treated J1-FL expressed in HEK293T cells (fig. S6B) samples gave a similar result to digested J1-WT expressed in HEK293T cells (fig. S6A). These data indicate that the low Notch activation associated with the T145N and N143A variants is caused by loss of the N-glycan attached to the JAG1 β5-6 loop and not due to indirect effects on folding of the apical region of the C2 domain during biosynthesis.

**Loss of the β5-6 glycan affects JAG1-mediated smooth muscle differentiation**

We chose vascular smooth muscle cells as a model system for screening for JAG1 functionality due to the involvement of this ligand in their recruitment and differentiation (*20*). Consistently, *JAG1* gene mutations are linked to most cases of Alagille syndrome, a congenital disease affecting the liver and the cardiac and skeletal systems and characterized by vascular abnormalities (*21*). JAG1 is known to induce vascular smooth muscle cells (VSMCs) to change from a synthetic to contractile phenotype in culture and increase their production of α-smooth muscle actin (α-SMA) (*22*, *23*). To test the ability of N-glycan variants to increase α-SMA production in human aortic smooth muscle cells, we cultured the cells for 5-6 days on plates coated with immobilized JAG1 variants and evaluated α-SMA production by immunofluorescence microscopy. Under the conditions used, α-SMA was detected in VSMCs plated on WT-J1 or J1-FL but not the N-glycan variant N143A or the negative control proteins (the F207A/E228K variant and IgG, which contains an Fc region but does not activate the Notch signalling pathway) (Fig. 3A).

We also subjected lysates from the cells cultured on the N-glycan variants to immunoblotting for α-SMA. Both J1-FL and J1-WT increased α-SMA accumulation above baseline amounts, with the J1-FL protein being a more potent inducer than J1-WT in this assay (Fig. 3B). N-glycan β5-6 variants T145N and N143A both failed to increase α-SMA in cells, showing amounts similar to those seen with the negative control proteins (Fig. 3B). The DSL N-glycan variant N217A, which showed activity similar to wild-type proteins in the reporter cell assays, showed intermediate activity for α-SMA induction in VSMCs, with less induction than the wild-type proteins but more than the negative control proteins. This differentiation assay therefore

recapitulated the results observed with Notch reporter cells, indicating that presence of the JAG1 β5-6 glycan was required for activating physiologically relevant amounts of Notch.

**Loss of the N-glycan reduces the interaction of JAG1 constructs with phospholipids**

The reduction in Notch activation associated with the β5-6 N-glycan variants was further investigated using molecular assays to probe its effect on the lipid and Notch-binding properties of JAG1. Given the known role of C2 domain apical loops in lipid binding (*10*), N-glycan variants were assessed for their ability to bind to liposomes using a flow cytometry–based assay. Each ligand (in the form of J1-WT or mutant variant) was coupled to Protein G fluorescent beads by its Fc tag and incubated with fluorescein-labelled phosphatidylcholine (PC)-rich liposomes. Flow cytometry was used to identify liposome-ligand complexes, and the results were reported as a percentage of liposomes engaged in complexes with J1-WT (Fig. 4, A and B). C2 glycan variants N143A and T145N both showed a significant decrease in binding compared to WT, whereas the DSL glycan variant N217A and S142N β5-6 loop variant bound liposomes indistinguishably from J1-WT. Similar data were obtained for liposomes enriched with the outer leaflet lipid sphingomyelin (SM) (Fig. 4, A and B). For both liposome compositions, reduced lipid binding by the C2 N-glycan variants was similar to that seen for the DSL-EGF3 (DE3) variant, which lacks the C2 domain, and the D140A/D144A variant, which has C2 domain substitutions that reduce $Ca^{2+}$ binding in the apical region and introduce loop flexibility (fig. S2A and B) (*7*). PNGase F–digested J1-WT samples were also tested in this assay and showed similar results to the C2 N-glycan variants (fig. S7, A and B).

Because the C2 domain also has a Notch-binding surface distant from the apical loops (Fig. 1B), Notch-ligand interactions were probed at two different concentrations of EGF11–13 ligand-

binding fragments from NOTCH1 and NOTCH2. N-glycan variants T145N and N143A were assayed alongside S142N, N217A (the DSL glycan variant), and NOTCH binding–defective variants F207A, F207A/E228K, and E228K (Fig. 4C and fig. S7C). T145N and N143A showed statistically significant differences in binding, albeit to a lesser degree than variants containing substitutions in the Notch-ligand interface. These results were recapitulated in a binding assay utilising HEK293T cells expressing complete mouse Notch1 (Fig. 4D). Neither the S142N amino acid substitution on the β5-6 loop, which retains the N-glycan, nor loss of the N-glycan in the DSL domain affected Notch binding in these assays. These data indicate that although the β5-6 loop is located away from the Notch-binding interface (Fig. 1B), the lack of C2 N-glycan does have some effect on the ability of JAG1 to bind Notch.

**Molecular dynamics simulations suggest a role for the N-glycan in determining JAG1 membrane orientation**

We used coarse-grained molecular dynamics (MD) simulations to examine membrane interactions of the nonglycosylated form of the JAG1 C2 domain. For these simulations, we used a bilayer of PC:PS (75:25), which mimics the conditions in our liposome assays. Initially, a density map of orientation and distance of the C2 domain away from the lipid membrane was generated (Fig. 5A). Multiple alternative binding poses were identified. Structures of a glycosylated form of the C2 domain and the Jagged1-Notch complex were overlaid to indicate positions of the C2 N-glycan, the DSL domain, (which contains one of the two key binding sites for Notch), and the ligand-binding portion of Notch. In all cases of binding poses identified with the exception of an intermediate mode (Fig. 5B), the presence of the C2 N-glycan, the DSL domain and EGF1-3 domains of the ligand, and/or the EGF8-12 repeats of Notch sterically

clashed with the membrane (Fig. 5C). The intermediate mode was converted to an atomistic model and simulated for another 200 ns to verify the intermediate nature of the interaction that was observed in the more approximate coarse-grained simulations. The mode was confirmed to be intermediate because the orientation of the C2 domain with respect to the membrane changed in less than 40 ns in all repeats. The simulations were also done with a different ganglioside-containing membrane PC:GM1:GM3 (90:5:5), resembling more closely the outer leaflet of a mammalian cell. Multiple binding poses were again identified, with one intermediate binding mode allowing an apical interaction between glycosylated ligand and membrane when in the Notch-bound state. The large number of different binding modes identified with the two membranes suggests the C2 domain itself does not dictate the ligand orientation at the membrane but is aided by the presence of the N-glycan and associated DSL EGF regions.

**Discussion**

Loss-of-function mutations that reduce Notch signalling have been associated with both aging and tumorigenic cells (*2*, *24*, *25*). We screened COSMIC variants of JAG1 for their ability to activate Notch to gain functional insights into the role of the C2 domain. Many variants showed loss of function, with the T145N variant being most notable in altering the N-glycosylation motif on a C2 lipid-binding loop. Although modification and extension of O-glycans is a well-recognised modulator of Notch activity (*26*), no critical role for an N-glycan has been reported. Comparative sequence analysis demonstrated high conservation of the C2 N-glycan motif in Jagged, but not Delta, ligands in higher metazoans, suggesting biological importance.

Functional analysis of C2 N-glycan variants using reporter cell lines and a Jagged-dependent smooth muscle differentiation assay demonstrated a large reduction in the Notch activation capability of variants with mutations at $Asn^{143}$. The effect of the N143A and N143Q mutations was of a similar magnitude to the T145N COSMIC variant and Notch binding–defective ligands with substitutions affecting site 2, the DSL-EGF11 ligand-receptor interface. Substantial loss of activity was not seen with the DSL variant N217A, wherein the only other N-glycosylation site within the ligand fragment was removed by amino acid substitution. Efficient posttranslational modification of the asparagine residue within the NxS/T sequon of the C2 or DSL domains of the J1-WT fragment was demonstrated by the reduction in molecular weight observed by SDS-PAGE in the variants in which the motif had been altered by mutagenesis (Fig. 1C and fig. S4A). Glycoproteomics analysis of J1-WT expressed in HEK293T cells identified the presence of a complex-type N-glycan at each site. Protein expressed in HEK293S cells contained oligomannose modifications as expected. Both forms showed similar amounts of activity in comparative reporter assays, suggesting that glycan occupancy is a greater factor for activity than subtle changes in glycan structure (fig. S5C).

N-glycosylation is known to be involved in protein folding and quality control of secretory pathway glycoproteins; however none of the C2 or DSL N-glycan variants showed poor cellular secretion in our expression system, suggesting that the lack of activity was not attributable to localised misfolding (*27*, *28*). Furthermore, the enzymatic removal of N-glycans from J1-WT proteins bearing structurally distinct glycans allowed testing of proteins that had trafficked through the secretory pathway and demonstrated Notch-activating capacity prior to glycan removal. Similar to the C2 N-glycan variants, digested material exhibited poor ability to activate

Notch, indicating that specific removal of N-glycans from natively-folded and active JAG1 fragments J1-WT and J1-FL is associated with loss of activity. These data argue against any major folding or trafficking functions for the C2 N-glycan and suggest a direct role for the N-glycan in JAG1-mediated Notch activation at the cell surface.

Given the known role of C2 domains in membrane binding, we measured the lipid-binding activity of the N-glycan variants and PNGase-digested forms of J1-WT. We used a flow cytometry–based assay, wherein avidity effects conferred to the Protein G beads by the ligand Fc tag facilitated interactions likely to be weak due to the relatively low hydrophobic character of the apical C2 loop sequences in Notch ligands (*8*, *29*, *30*). Both the C2 N-glycan variants, but not the DSL variant, showed a statistically significant reduction in binding to PC-rich liposomes, as did the PNGase-digested forms. N-glycan variants were also tested with liposomes containing SM, an outer leaflet lipid, which gave similar results to PC-rich liposomes suggesting that the presence of the C2 N-glycan is important for JAG1 membrane binding. The N-glycan variants were also observed to have some detrimental effect on binding to complete Notch1 expressed in HEK293T cells or the EGF11-13 fragments of NOTCH1/2 despite the location of the β5-6 loop (and glycan) away from the Notch binding surface. These are likely to be indirect effects, because they were of lower magnitude than those observed for Notch interface variants, such as F207A/E228K. It is notable that most of the in vitro–evolved high affinity ligand variants utilised to obtain structures of receptor-ligand complexes contain amino acid substitutions away from the binding interface (*12*). These either occurred in loops or core β-strands, or affected the C2-DSL domain interface, indicating that indirect effects can modulate Notch binding.

Previous structures of JAG1 either in the presence or absence of Notch lacked the N-glycan that we observed (*7*, *12*). This is due to the method of production and/or preparation of the material used for crystallography, wherein the sugars are often trimmed or removed. Two crystal structures exist for JAG2 and fly Delta in which the N-glycan is present on the β5-6 loop and can be used to aid modelling (Fig. 1B) (*12*, *16*). A possible effect of the N-glycan might be to stabilise the β5-6 loop, given that it was noted that α(1,6)-linked fucose (located at the reducing-end *N*-acetylglucosamine residue linked to the peptide in complex-type glycans) interacted with a W151 side chain of the loop in JAG2 (*12*). In the crystal structure of the holo form of isolated JAG1 that lacked the N-glycan, it was observed that even in the presence of $Ca^{2+}$ the apical loops were still mobile, giving rise to different coordination shells within crystallographically-independent molecules (*12*). The N-glycan, which is attached to $Asn^{143}$, adjacent to the $Ca^{2+}$ ligand $Asp^{144}$, may interact with the base of the β5-6 loop to reduce loop flexibility, facilitate coordination of $Ca^{2+}$, and promote interactions with lipid. A $Ca^{2+}$ bound to the apical region of the C2 domain of Phospholipase A2α is shown to bridge to the DHPC phosphate group in a high resolution lipid-bound structure (*10*). This might explain the conservation of the N-glycan because $Ca^{2+}$ binding to the C2 domains of Notch ligands is specific to the Jagged/Serrate family. We also noted that the tetra-antennary form of the complex-type glycan (and the oligomannose form) attached to the β5-6 loop was in proximity to the cationic β-groove, identified in some other C2 domains as important for lipid interactions (*31*). Therefore, in addition to stabilisation of the β5-6 loop region, it is possible that the N-glycan confers steric constraints on the ligand-membrane interaction.

Molecular dynamics simulations were used to further explore the potential orientations of the JAG1 C2 domain with the membrane and showed that many different binding poses were possible. These data are reminiscent of the C2 domain of SHIP2 (SH2-containing inositol 5 phosphatase 2) (*32*) and suggest that the N-glycan and covalently attached domains may co-operate with the lipid-binding module to dictate the membrane orientation. This is not unexpected, because the JAG1 C2 apical loops implicated in binding show weak hydrophobic character. Given the clear reduction in liposome binding observed for ligand variants lacking the C2 glycan, these data suggest that the sugar may stabilise the β5-6 lipid-binding loop and aid the JAG1 C2 domain in finding the optimal binding mode with the membrane.

Because the apical loops known to be directly involved in lipid binding differ in length, sequence, and $Ca^{2+}$ coordination between the two Notch ligand families, our data do not rule out a role for the N-glycan in conferring specificity for certain lipids, especially when taking into account previous observations of ligand-specific differences in comparative liposome-binding experiments (*8*). Different lipid-binding properties may reflect the varied physiological settings in which Notch signalling operates and the requirement for different mechanisms to fine-tune what is a relatively simple signal transduction pathway. However, our functional studies, combined with molecular dynamics simulations, suggest that for JAG1, the presence of an N-glycan on the apical loop of the C2 domain may be required to promote a particular orientation of the ligand at the membrane, either to facilitate cis or trans interactions with Notch, to promote interactions with other membrane components, or to enable protease-mediated Notch cleavage to occur under different physiological conditions (shear or pulling forces). A recent cross-linking study identified additional Jag1 C2 interactions with the membrane-proximal NRR region of

Notch, suggesting that a specific ligand orientation at the membrane may be important not only for interactions with the core ligand-binding sites but also for other regions of the receptor previously thought to be more distally located (*33*).

In summary, our molecular, cellular, and computational analyses have identified a previously unrecognised role for an N-glycan on the C2 domain in facilitating JAG1 interactions at the cell membrane, which are essential for Notch activation. The conservation of the N-glycosylation site in Jagged/Serrate, but not Delta, ligands suggests that other Jagged paralogues have a similar requirement. These data emphasise the importance of ligand-specific posttranslational modifications in the generation of the Notch signal.

## Materials and Methods

### Protein expression and purification

Ligand proteins, spanning from the N-terminus to EGF3, were produced as C-terminal Fc-and His-tagged dimer constructs in human embryonic kidney HEK293T or HEK293S cells by a transient transfection approach (*34*) and were purified as previously described (*7*). Notch1/2 EGF11-13 constructs were expressed as C-terminal BirA- and His-tagged recombinant constructs in S2 insect cells and purified as previously described (*8*).

### Sequence Alignment

Amino acid sequences of Notch ligands from different species were obtained from UniProt and aligned using Clustal Omega.

**Notch activation assays**

Purified ligand Fc-tagged constructs (10 μg/mL in HBS buffer containing 200 mM HEPES, 150 mM NaCl, 0.9 mM $CaCl_2$, pH = 7.4) were immobilized on 96-well tissue culture plates overnight at 4 °C. Equivalent immobilization was confirmed using anti-His tag antibody (ab1187; Abcam, UK) and 65D JAG1 mAb (*35*). The plates were washed once with HBS buffer and Notch split luciferase reporter cells (HEK293T cells stably expressing mouse Notch1/2-NLuc and CLuc-RBPjk) or CHO-YFP reporter cells (CHO-K1 cells stably expressing human NOTCH1(ECD)-Gal4 and H2B-YFP controlled by a UAS promoter (*36*)) were seeded onto the immobilised ligand ($4 \times 10^4$ cells of mN1-NLuc/CLuc-RBPjk, $1 \times 10^5$ mN2-NLuc/CLuc-RBPjk or $4 \times 10^4$ cells of CHO-YFP reporter cells each well).

Luciferin signal of Notch luciferase reporter cells was measured after 24 hours culture by Tristar LB941 (Berthold Technologies) as previously described (*37*). YFP signal of CHO-YFP reporter cells was measured after 48 hours culture by analysis of 10,000 single cells using BD LSRFortessa™ X20 flow cytometer system (excitation 488 nm, emission 530 nm). Data were analysed using FlowJo™10.

**Smooth muscle differentiation assay**

Human aortic smooth muscle cells (hAoSMCs) (Lonza) were bought at passage 3. Cells were cultured in smooth muscle basal medium (SmBM, Lonza) supplemented with growth supplement (SmGM™-2 SingleQuots™, Lonza), and passaged at 80% confluence. Cells were used at passage five and six. For the differentiation assay, 6-well plates were coated with recombinant

protein G (50µg/mL) (Pierce™, Thermo Fisher Scientific) overnight at room temperature and subsequently blocked with bovine serum albumin (BSA) (1% in PBS) for 1 h against non-specific binding. For immunocytochemistry, 13mm glass coverslips were pre-treated with poly-L-lysine (0.01%) (Merck) prior to protein G coating for protein adhesion. Purified J1 ligand dimers (10 nM in PBS with 0.1% BSA) together with Recombinant Human JAG1 Fc Chimera Protein (J1-FL), CF (1277-JG-050) and Recombinant Human IgG1 Fc Protein, CF (110-HG-100) obtained from R & D were coated on plates overnight at 4°C. After three times washing with PBS, cells (approximately 2500 cells/cm$^2$) were cultured on the plate for 5-6 days, and the media was changed every other day. Differentiation to a contractile phenotype was assessed by detecting alpha-smooth muscle actin (α-SMA) production by western blot/immunofluorescent microscopy. β-tubulin (D3U1W) mouse mAb (1:1000) (Cell Signaling Technology) and α-SMA (D4K9N) XP® rabbit mAb (1:1000) (Cell Signaling Technology) were used to detect signal of β-tubulin and α-SMA in western blotting. α-SMA (1:200), anti-rabbit-AF546 (1:400) (Invitrogen), phalloidin-AF633 (1:50) (Invitrogen) and VECTASHIELD® antifade mounting media with DAPI (Vector Laboratories) were used to detect α-SMA, F-actin and nuclear DNA by immunofluorescent microscopy.

**Glycoproteomics**

Approximately 5µg sample was reduced, loaded and run on an SDS-PAGE. Gel bands were excised and washed sequentially with HPLC grade water followed by 1:1 (v/v) MeCN/$H_2O$. Gel bands were dried (using a vacuum centrifuge), treated with 10mM dithiothreitol (DTT) in 100mM $NH_4HCO_3$ and incubated for 45 minutes at 56°C with shaking. DTT was removed and 55mM iodoacetamide (in 100mM $NH_4HCO_3$) was added and incubated for 30 minutes in the

dark. All liquid was removed and gels were washed with 100mM $NH_4HCO_3$/MeCN as above. Gels were dried and 12.5 ng/µL trypsin, chymotrypsin or alpha lytic protease was added separately and incubated overnight at 37°C. Samples were then washed and (glyco)peptides were extracted and pooled with sequential washes with 5% (v/v) formic acid (FA) in $H_2O$ and MeCN. Dried samples were reconstituted in 0.05% trifluoroacetic acid and run by LC-MS. Samples were analysed using an Ultimate 3000 UHPLC coupled to an Orbitrap Fusion Tribrid mass spectrometer (Thermo Fisher Scientific). Tryptic peptides were loaded onto a 75 µm × 2 cm pre-column and separated on a 75 µm × 15 cm Pepmap C18 analytical column (Thermo Fisher Scientific). Buffer A was 0.1% FA in $H_2O$ and buffer B was 0.1% FA in 80% MeCN with 20% $H_2O$. A 40min linear gradient (0% to 40% buffer B) was used. Data was collected in data-dependent acquisition mode with a mass range 330 to 2000 m/z and at a resolution of 120000. For MS/MS scans, HCD normalized energy was set to 30%. Glycopeptide data was analysed with Byonic and output files were imported into Byologic for quantification (Protein Metrics). A minimum Byonic threshold score of 100 was used for glycopeptide identification. All glycopeptide assignments were manually validated. For quantification, the extracted ion chromatogram intensities for each glycopeptide and unoccupied peptides were summed and plotted relative to the total intensity for each glycosite. The Fc N-glycan (in the Fc domain of the J1-WT construct used) was detected but not included in the full analysis.

**PNGase F digestion of Notch ligands**

Deglycosylation of ligand proteins was performed under non-denaturing reaction conditions by PNGase F (NEB, P0704, 500,000 units/mL). 2-10 µg of purified Notch ligand was combined with 1:1 w/v of 10X GlycoBuffer 2 (1X GlycoBuffer 2: 50 mM Sodium Phosphate, pH 7.5 at

25°C) and $H_2O$ (if necessary) to make a total reaction volume with 100 ng/μL ligand protein. 10:1 w/v of PNGase F (5000 units/mL) was added per reaction and incubated at 37°C for 4-24 hours. An aliquot of the purified Notch ligand was subjected to the non-denaturing reaction conditions without adding PNGase F to provide a positive control for the fully deglycosylated ligand. After incubation, the extent of deglycosylation was assessed by mobility shifts on SDS-PAGE gels.

**Notch binding assays**

Notch binding assays were performed as previously described using purified Fc-tagged ligand constructs (J1-WT and mutant variants) and biotinylated NOTCH1/2 EGF11-13 constructs (*8*). Pierce™ 96-well clear nickel-coated plates (Thermo Scientific) were coated with 5 μg/mL purified J1-WT and mutant variants in 100 μL 20 mM HEPES pH 7.4 containing 200 mM NaCl and 5 mM $CaCl_2$ (HBS). After incubating at 4 °C overnight, the plate was washed 3 times with 200 μL HBS and blocked with 4% (w/v) bovine serum albumin (BSA, Sigma) in the same buffer for 1 hour at room temperature. NOTCH1 and NOTCH2 EGF11-13 constructs that had been biotinylated by site-specific biotin ligase (Avidity BirA-500 kit) were mixed at a 4:1 molar ratio to NeutrAvidin-HRP (Life Technologies) in HBS for 1 hour on a rotor at room temperature. After the plate blocking step, three x 200 μL HBS washes were performed to remove remaining BSA. The pre-clustered Notch constructs at 400 nM and 40 nM (NOTCH1) and 250 nM and 20 nM (NOTCH2) in 50 μL HBS were then added to the ligand-coated plates and incubated for 1.5 hour at room temperature. After 4x200 μL washes with HBS containing 0.05% (v/v) Tween-20, followed by 2x200 μLwashes with HBS, the plate was developed with 2,20-Azino-bis(3-

ethylbenzothiazoline-6-sulphonic acid) diammonium salt (Sigma-Aldrich). Absorbance was measured with a PHERAstar FS microplate reader (BMG LABTECH) at a wavelength of 415 nm. Data from variants were expressed relative to WT signal and plotted using Prism 9.

For binding experiments performed with HEK293T cells expressing complete full length Notch1 , 50nM J1-FL, J1-WT and mutant variant ligands and 25 nM anti-human/AF488 antibody (for 2:1 clustering) were conjugated in PBS by rotating at cold for1 hour. 200,000 cells were blocked in growth media supplemented with 1% BSA and 10% goat serum for 45 minutes at 37°C. The ligand solution was added at 1:5 ratio directly into the blocking medium (final ligand concentration: 10nM) and incubated for 2 hours at 37°C. The cells were collected and washed 3 times with HEPES BSS and analysed withFACS. The data were analysed with FlowJo™10.

**FACS-based liposome aggregation assay**

Chloroform lipid solutions (Avanti Polar lipids, US) were mixed in desired ratios (PC-rich liposome: POPC:DOPS:PE-CF (70:25:5), SM-rich liposome: POPC:SM:DOPS:PE-CF (30:40:25:5)) and first dried under nitrogen and then placed in a freezer dryer for 1 hour in the dark. Dried lipids were resuspended in HBS buffer (20 mM HEPES, 200 mM NaCl, 5 mM $CaCl_2$, pH 7.4) at a final concentration of 2 mM in a shaker for one hour in the dark at room temperature before aliquoting. Aliquots of lipid stock were frozen in liquid nitrogen and then thawed in a 37°C water bath (for ~ 3 minutes), and this freeze-thaw cycle was repeated 8 times. After the last freezing step, aliquots were stored at -80°C until use. One lipid aliquot was thawed at room temperature and extruded with 21 passes through a polycarbonate Nucleopore membrane (Whatman®, 100 nm pore width) on the day of the assay. The size/homogeneity of the liposomes was confirmed using dynamic light scattering.

Protein G-coated fluorescent bead solution (SPHERO$^{TM}$, 5.88 μm, PAK blue, 10 μL per reaction) was washed 2 times with 10 volumes of HBS/BSA (20 mM HEPES, 200 mM NaCl, 5 mM $CaCl_2$, pH 7.4 containing 3% lipid- free bovine serum albumin (w/v)) and resuspended with 5 volumes of HBS/BSA. 2 μg purified Notch ligand or mouse IgG was added per reaction and kept at 4°C overnight in the dark or on ice for 1hr. For liposome binding of PNGase-treated samples, digestion was carried out on ligand bound to beads according to the following. 0.2 μL PNGase F (NEB, P0704, 500,000 units/mL) was added per reaction and incubated at 37°C for 4 hours in the dark. The respective control reactions were also incubated at 37°C for 4 hours in the dark without adding PNGase F. After incubation, the PNGase F digestion was quenched by chilling the reaction mix on ice. Ligand-coated protein G beads were washed once with 100 μL HBS/BSA buffer per reaction and resuspended in 50 μL ice-cold HBS buffer. 2 mM liposome stock was diluted 400-fold with HBS buffer before adding into beads solution (50 μL diluted liposome solution per reaction). After 30 minutes incubation of beads and liposomes mixture on ice in the dark, 200 μL of HBS was added to each reaction before analysis by BDX-20 (BD Biosciences) flow cytometer (excitation/emission at 488 nm/530 nm (liposomes) and 640 nm/670 nm (Protein G beads)).

**Molecular Dynamics**

MD simulations were run using a previously described protocol (*32*). All steps are described below.

**Coarse-grained molecular dynamics (MD) simulations**

Coarse-grained MD simulations were performed in GROMACS 2018.6 (*38*) with the Martini 2.2 force field (*39*). The input structure (*7*) was truncated to only contain the N-terminal C2 domain (residues 32 to 188) using PyMOL (The PyMOL Molecular Graphics System, version 2.0 Schrödinger, LLC), and missing residues were added with Modeller (*40*). The truncated structure was coarse-grained using the Martinize script (*39*) with default elastic network parameters to restrain secondary and tertiary structure. The protein was solvated and positioned above a POPC:DOPS (molar ratio 75:25) lipid membrane using the Insane script (*41*) with a box size of 7x7x18 $nm^3$. The protein was placed at a minimum distance of 4.4 nm above the membrane, which is four times the VDW and electrostatic cutoff distances of 1.1 nm. 10% antifreeze water was added (*42*) and the system was neutralised with sodium ions. The protein was rotated through a random angle relative to the membrane to avoid bias in the binding orientation. The system was then minimised and equilibrated. During equilibration, a restraint was applied to ensure that the protein could only encounter the upper leaflet of the membrane. This was a PLUMED UPPER_WALLS (*43*) restraint, with a protein to lipid centre-of-mass distance of 7 nm and with an energy constant of k = 50 (internal units of the PLUMED code). Equilibration was run in the NPT ensemble with a semi-isotropic Berendsen barostat (*44*) and time constant of 14 ps, keeping pressure at 1 bar, and at v-rescale temperature coupling applied separately to lipids, protein and solvent, with a time constant of 1 ps to keep temperature at 323 K. Equilibration was run with 20 fs time steps for 10 ns. Production runs had the same settings, but with 35 fs time steps and was run for 2000 ns. 25 independent repeats were made. The same set of simulations were performed with a POPC:DPG1:DPG3 (molar ratio 90:5:5) lipid membrane.

**Generating Distance vs. $R_{zz}$ Plots**

Distances between the centre of mass of the protein and the centre of mass of the lipids were calculated for each frame using gmx distance (after centering the protein in the box). The final frame of the first repeat was used as reference frame to calculate the rotation matrix, R. $R_{zz}$ is the zz component of this matrix. The reference frame has $R_{zz} = 1.0$ per definition. The rotation matrix was calculated using gmx rotmat, after xy plane fitting. Plotting was done in Python 3 with Numpy (*45*) and Matplotlib (*46*) packages.

**Atomistic simulations**

One frame from the simulations with the POPC:DOPC lipid membrane was refined with atomistic simulations. Frame 237 of repeat 21 (snapshot after 79 ns), which represents a physically positive but intermediate binding mode, was converted from coarse-grained to atomistic resolution (force field charm36m (*47*, *48*), and TIP3P water), using CG2AT (*49*). Atomistic simulations were run with GROMACS 2018.6 (*38*). The system was first minimised, then equilibrated for 10 ps in the NVT ensemble and 40 ps in the NPT ensemble. The equilibrated system was run for 200 ns. Both equilibration and production used 2 fs timesteps with 1.2 nm VDW and electrostatic cutoff distance, v-rescale temperature coupling with a temperature of 300 K and timeconstant of 0.1 ps independently kept for protein, lipids and solvent (incl. ions). A Parrinello-Rahman barostat (*50*) was applied to the NPT equilibration and production run with semi-isotropic pressure coupling, keeping pressure at 1 bar with time constant of 5 ps and water compressibility of $4.5 \cdot 10^{-5}$ bar. Long-range electrostatics were

handled using the particle mesh Ewald method (*51*). Three repeats were made of the atomistic simulations, starting from the minimisation step.

**Reproducibility**

All scripts for reproducing the simulations are available at https://github.com/andreashlarsen/Meng2022-Jagged_C2

**Statistical analysis**

Statistical data were analysed with Prism 9 (GraphPad, San Diego, CA, USA). Parametric and non-parametric tests used are indicated in each figure legend, together with (where appropriate) the post-hoc test used for multiple comparison. Values are presented with the mean ± SD. All flow cytometry data were analysed with FlowJo™10 (BD Life Sciences, USA).

**Supplementary Materials**

Figs. S1 to S7.

**References and Notes**


1. S. J. Bray, Notch signalling in context. *Nat. Rev. Mol. Cell Biol.* **17**, 722–735 (2016).
2. C. S. Nowell, F. Radtke, Notch as a tumour suppressor. *Nat. Rev. Cancer*. **17** (2017), pp. 145–159.
3. C. Siebel, U. Lendahl, Notch signaling in development, tissue homeostasis, and disease. *Physiol. Rev.* **97**, 1235–1294 (2017).

4. W. R. Gordon, D. Vardar-Ulu, G. Histen, C. Sanchez-Irizarry, J. C. Aster, S. C. Blacklow, Structural basis for autoinhibition of Notch. *Nat. Struct. Mol. Biol. 2007 144*. **14**, 295–300 (2007).

5. R. A. Kovall, S. C. Blacklow, Mechanistic Insights into Notch Receptor Signaling from Structural and Biochemical Studies. *Curr. Top. Dev. Biol.* **92**, 31–71 (2010).

6. B. D. Giaimo, E. K. Gagliani, R. A. Kovall, T. Borggrefe, Transcription Factor RBPJ as a Molecular Switch in Regulating the Notch Response. *Adv. Exp. Med. Biol.* **1287**, 9–30 (2021).

7. C. R. Chillakuri, D. Sheppard, M. Xenia, G. Ilagan, L. R. Holt, F. Abbott, S. Liang, R. Kopan, P. A. Handford, S. M. Lea, Structural Analysis Uncovers Lipid-Binding Properties of Notch Ligands. *CellReports*. **5**, 861–867 (2013).

8. R. J. Suckling, B. Korona, P. Whiteman, C. Chillakuri, L. Holt, P. A. Handford, S. M. Lea, Structural and functional dissection of the interplay between lipid and Notch binding by human Notch ligands. *EMBO J.* **36**, 2204–2215 (2017).

9. N. J. Kershaw, N. L. Church, M. D. W. Griffin, C. S. Luo, T. E. Adams, A. W. Burgess, Notch ligand delta-like1: X-ray crystal structure and binding affinity. *Biochem. J.* **468**, 159–166 (2015).

10. Y. Hirano, Y. G. Gao, D. J. Stephenson, N. T. Vu, L. Malinina, D. K. Simanshu, C. E. Chalfant, D. J. Patel, R. E. Brown, Structural basis of phosphatidylcholine recognition by the C2-domain of cytosolic phospholipase A2α. *Elife*. **8** (2019), doi:10.7554/eLife.44760.

11. V. C. Luca, K. M. Jude, N. W. Pierce, M. V. Nachury, S. Fischer, K. C. Garcia, Structural basis for Notch1 engagement of Delta-like 4. *Science (80-. ).* **347**, 847–853 (2015).

12. V. C. Luca, B. C. Kim, C. Ge, S. Kakuda, D. Wu, M. Roein-Peikar, R. S. Haltiwanger, C.

Zhu, T. Ha, K. C. Garcia, Notch-Jagged complex structure implicates a catch bond in tuning ligand sensitivity. *Science (80-. ).* **355**, 1320–1324 (2017).

13. A. Pandey, N. Niknejad, H. Jafar-Nejad, Multifaceted regulation of Notch signaling by glycosylation. *Glycobiology*. **31**, 8–28 (2021).

14. R. A. Kovall, B. Gebelein, D. Sprinzak, R. Kopan, The Canonical Notch Signaling Pathway: Structural and Biochemical Insights into Shape, Sugar, and Force. *Dev. Cell* (2017), , doi:10.1016/j.devcel.2017.04.001.

15. S. Kakuda, R. S. Haltiwanger, Deciphering the Fringe-Mediated Notch Code: Identification of Activating and Inhibiting Sites Allowing Discrimination between Ligands. *Dev. Cell*. **40**, 193–201 (2017).

16. T. Martins, Y. Meng, B. Korona, R. Suckling, S. Johnson, P. A. Handford, S. M. Lea, S. J. Bray, The conserved C2 phospholipid-binding domain in Delta contributes to robust Notch signalling. *EMBO Rep.*, e52729 (2021).

17. S. A. Forbes, D. Beare, H. Boutselakis, S. Bamford, N. Bindal, J. Tate, C. G. Cole, S. Ward, E. Dawson, L. Ponting, R. Stefancsik, B. Harsha, C. Yin Kok, M. Jia, H. Jubb, Z. Sondka, S. Thompson, T. De, P. J. Campbell, COSMIC: somatic cancer genetics at high-resolution. *Nucleic Acids Res.* **45**, 777–783 (2016).

18. J. Cordle, S. Johnson, J. Zi, Y. Tay, P. Roversi, M. Wilkin, B. Hernandez-Diaz, H. Shimizu, S. Jensen, P. Whiteman, B. Jin, C. Redfield, M. Baron, S. M. Lea, P. A. Handford, A Conserved Face of the Jagged/Serrate DSL Domain is Involved in Notch Trans-Activation and Cis-Inhibition. *Nat. Struct. Mol. Biol.*, 849–857 (2008).

19. P. Whiteman, P. A. Handford, Defective secretion of recombinant fragments of fibrillin-1: implications of protein misfolding for the pathogenesis of Marfan syndrome and related

disorders. *Hum. Mol. Genet.* **12**, 727–737 (2003).

20. L. J. Manderfield, F. A. High, K. A. Engleka, F. Liu, L. Li, S. Rentschler, J. A. Epstein, Notch activation of Jagged1 contributes to the assembly of the arterial wall. *Circulation*. **125**, 314–323 (2012).

21. F. A. High, M. M. Lu, W. S. Pear, K. M. Loomes, K. H. Kaestner, J. A. Epstein, Endothelial expression of the Notch ligand Jagged1 is required for vascular smooth muscle development. *Proc. Natl. Acad. Sci. U. S. A.* **105**, 1955–9 (2008).

22. S. Loerakker, O. M. J. A. Stassen, F. M. Ter Huurne, M. Boareto, C. V. C. Bouten, C. M. Sahlgren, Mechanosensitivity of Jagged-Notch signaling can induce a switch-type behavior in vascular homeostasis. *Proc. Natl. Acad. Sci. U. S. A.* **115**, E3682–E3691 (2018).

23. Y. Xia, A. Bhattacharyya, E. E. Roszell, M. Sandig, K. Mequanint, The role of endothelial cell-bound Jagged1 in Notch3-induced human coronary artery smooth muscle cell differentiation. *Biomaterials*. **33**, 2462–2472 (2012).

24. I. Martincorena, J. C. Fowler, A. Wabik, A. R. J. Lawson, F. Abascal, M. W. J. Hall, A. Cagan, K. Murai, K. Mahbubani, M. R. Stratton, R. C. Fitzgerald, P. A. Handford, P. J. Campbell, K. Saeb-Parsy, P. H. Jones, Somatic mutant clones colonize the human esophagus with age. *Science*. **362**, 911–917 (2018).

25. Y. Gao, L. Bai, G. Shang, Notch-1 promotes the malignant progression of osteosarcoma through the activation of cell division cycle 20. *Aging (Albany. NY).* **13**, 2668–2680 (2020).

26. S. Varshney, P. Stanley, Multiple roles for O-glycans in Notch signalling. *FEBS Lett.* **592**, 3819–3834 (2018).

27. H. Yagi, M. Yagi-Utsumi, R. Honda, Y. Ohta, T. Saito, M. Nishio, S. Ninagawa, K. Suzuki, T. Anzai, Y. Kamiya, K. Aoki, M. Nakanishi, T. Satoh, K. Kato, Improved secretion of glycoproteins using an N-glycan-restricted passport sequence tag recognized by cargo receptor. *Nat. Commun. 2020 111*. **11**, 1–9 (2020).

28. H. DN, L. L, P. ET, K. JW, The intrinsic and extrinsic effects of N-linked glycans on glycoproteostasis. *Nat. Chem. Biol.* **10**, 902–910 (2014).

29. O.-H. Shin, J. Lu, J.-S. Rhee, D. R. Tomchick, Z. P. Pang, S. M. Wojcik, M. Camacho-Perez, N. Brose, M. Machius, J. Rizo, C. Rosenmund, T. C. Südhof, Munc13 C2B domain is an activity-dependent Ca2+ regulator of synaptic exocytosis. *Nat. Publ. Gr.* **17** (2010), doi:10.1038/nsmb.1758.

30. E. Connell, P. Scott, B. Davletov, Real-time assay for monitoring membrane association of lipid-binding domains. *Anal. Biochem.* **377**, 83–88 (2008).

31. W. Cho, R. V. Stahelin, Membrane binding and subcellular targeting of C2 domains. *Biochim. Biophys. Acta - Mol. Cell Biol. Lipids*. **1761**, 838–849 (2006).

32. A. H. Larsen, M. S. P. Sansom, Binding of Ca2+-independent C2 domains to lipid membranes: A multi-scale molecular dynamics study. *Structure* (2021), doi:10.1016/J.STR.2021.05.011.

33. M. R. Zeronian, O. Klykov, J. Portell I de Montserrat, M. J. Konijnenberg, A. Gaur, R. A. Scheltema, B. J. C. Janssen, Notch-Jagged signaling complex defined by an interaction mosaic. *Proc. Natl. Acad. Sci. U. S. A.* **118** (2021), doi:10.1073/pnas.2102502118.

34. A. R. Aricescu, W. Lu, E. Y. Jones, A time- and cost-efficient system for high-level protein production in mammalian cells. *Acta Crystallogr. Sect. D Biol. Crystallogr.* **62**, 1243–1250 (2006).

35. M. Masiero, D. Li, P. Whiteman, C. Bentley, J. Greig, T. Hassanali, S. Watts, S. Stribbling, J. Yates, E. Bealing, J. L. Li, C. Chillakuri, D. Sheppard, S. Serres, M. Sarmiento-Soto, J. Larkin, N. R. Sibson, P. A. Handford, A. L. Harris, A. H. Banham, Development of Therapeutic Anti-JAGGED1 Antibodies for Cancer Therapy. *Mol. Cancer Ther.* **18**, 2030–2042 (2019).

36. D. Sprinzak, A. Lakhanpal, L. Lebon, L. A. Santat, M. E. Fontes, G. A. Anderson, J. Garcia-Ojalvo, M. B. Elowitz, Cis-interactions between Notch and Delta generate mutually exclusive signalling states. *Nature*. **465**, 86–91 (2010).

37. M. X. G. Ilagan, S. Lim, M. Fulbright, D. Piwnica-Worms, R. Kopan, Real-time imaging of Notch activation with a luciferase complementation-based reporter. *Sci. Signal.* **4** (2011), doi:10.1126/scisignal.2001656.

38. M. J. Abraham, T. Murtola, R. Schulz, S. Páll, J. C. Smith, B. Hess, E. Lindah, GROMACS: High performance molecular simulations through multi-level parallelism from laptops to supercomputers. *SoftwareX*. **1**–**2**, 19–25 (2015).

39. D. H. De Jong, G. Singh, W. F. D. Bennett, C. Arnarez, T. A. Wassenaar, L. V. Schäfer, X. Periole, D. P. Tieleman, S. J. Marrink, Improved parameters for the martini coarse-grained protein force field. *J. Chem. Theory Comput.* **9**, 687–697 (2013).

40. A. Fiser, R. K. G. Do, A. Šali, Modeling of loops in protein structures. *Protein Sci.* **9**, 1753–1773 (2000).

41. T. A. Wassenaar, H. I. Ingólfsson, R. A. Böckmann, D. P. Tieleman, S. J. Marrink, Computational lipidomics with insane: A versatile tool for generating custom membranes for molecular simulations. *J. Chem. Theory Comput.* **11**, 2144–2155 (2015).

42. S. J. Marrink, H. J. Risselada, S. Yefimov, D. P. Tieleman, A. H. De Vries, The

MARTINI Force Field: Coarse Grained Model for Biomolecular Simulations. *J. Phys. Chem. B*. **111**, 7812–7824 (2007).

43. G. A. Tribello, M. Bonomi, D. Branduardi, C. Camilloni, G. Bussi, PLUMED 2: New feathers for an old bird. *Comput. Phys. Commun.* **185**, 604–613 (2014).

44. H. J. C. Berendsen, J. P. M. Postma, W. F. Van Gunsteren, A. Dinola, J. R. Haak, Molecular dynamics with coupling to an external bath. *J. Chem. Phys.* **81**, 3684 (1998).

45. C. R. Harris, K. J. Millman, S. J. van der Walt, R. Gommers, P. Virtanen, D. Cournapeau, E. Wieser, J. Taylor, S. Berg, N. J. Smith, R. Kern, M. Picus, S. Hoyer, M. H. van Kerkwijk, M. Brett, A. Haldane, J. F. del Río, M. Wiebe, P. Peterson, P. Gérard-Marchant, K. Sheppard, T. Reddy, W. Weckesser, H. Abbasi, C. Gohlke, T. E. Oliphant, Array programming with NumPy. *Nature*. **585**, 357–362 (2020).

46. J. D. Hunter, Matplotlib: A 2D graphics environment. *Comput. Sci. Eng.* **9**, 90–95 (2007).

47. R. B. Best, X. Zhu, J. Shim, P. E. M. Lopes, J. Mittal, M. Feig, A. D. MacKerell, Optimization of the additive CHARMM all-atom protein force field targeting improved sampling of the backbone φ, ψ and side-chain χ1 and χ2 Dihedral Angles. *J. Chem. Theory Comput.* **8**, 3257–3273 (2012).

48. J. Huang, S. Rauscher, G. Nawrocki, T. Ran, M. Feig, B. L. De Groot, H. Grubmüller, A. D. MacKerell, CHARMM36m: an improved force field for folded and intrinsically disordered proteins. *Nat. Methods*. **14**, 71–73 (2017).

49. O. N. Vickery, P. J. Stansfeld, CG2AT2: An Enhanced Fragment-Based Approach for Serial Multi-scale Molecular Dynamics Simulations. *J. Chem. Theory Comput.* **17**, 6472–6482 (2021).

50. M. Parrinello, A. Rahman, Polymorphic transitions in single crystals: A new molecular

dynamics method. *J. Appl. Phys.* **52**, 7182 (1998).

51. T. Darden, D. York, L. Pedersen, Particle mesh Ewald: An N·log(N) method for Ewald sums in large systems. *J. Chem. Phys.* **98**, 10089 (1998).

**Acknowledgments:** We thank A. Davies for assistance with COSMIC variant cloning and purification. We thank Kati Kemppainen for technical guidance and insightful comments. We are grateful to Rafi Kopan and David Sprinzak for Notch reporter reagents. We thank Christina Redfield for critical reading of the manuscript.

**Funding:** This was supported by MRC grant MR-R009317-1 and MR-V008935-1 awarded to PAH as well as InFLAMES Flagship Programme of the Academy of Finland (decision number: 337530) (CS, SS), and the Academy of Finland (decision number: 316882, 330411, 307133) (CS, SS). AHL was supported by the Carlsberg Foundation, grant CF19-0288. YM was supported by a St Catherine's College, Oxford, Overseas Scholarship. WBS and SAB are supported by funding from the UK Research and Innovation (UKRI) Future Leaders Fellowship [grant number MR/V02213X/1], Cellular imaging was performed in Cell Imaging and Cytometry Core, Turku Bioscience, Turku, Finland, supported by Biocenter Finland.

**Author contributions:** YM and PAH designed research, YM, SS, SJ, SM, XF, WBS, SAB, AL performed research. WBS, SS, CS, AL, MS contributed new reagents/analytical tools, YM, WBS, SS, AL, CS, MS, PAH analysed data. YM and PAH wrote first draft of manuscript to which all other authors contributed.

**Competing Interests:** The authors declare that they have no competing interests.

**Data and materials availability:** The mass spectrometry raw data and Byonic output files have been deposited in the ProteomeXchange Consortium via the PRIDE (*52*) repository with the dataset identifier PXD034133. All other data needed to evaluate the conclusions in the paper are present in the paper or the Supplementary Materials.

**License:** For the purpose of open access, the author(s) has applied a Creative Commons Attribution (CC BY) licence to any Author Accepted Manuscript version arising.

**Figure legends**

**Fig. 1. An N-glycan site is conserved in the Jagged/Serrate family of Notch ligands.** (**A**) Amino acid sequence alignment of the C2 domain β5-6 loop region of human Jagged1 (JAG1) with other Jagged, Serrate (SER), Delta (DEL), and Delta-like (DLL) ligands indicating conservation of the N-glycan motif in Jagged/Serrate (red) but not Delta ligands (blue). The asparagine of the NxS/T motif highlighted in pink. (**B**) Structure of JAG1 with $Asn^{143}$ (N143) and $Asn^{217}$ (N217) highlighted in pink. C2 domain, cyan; DSL domain, orange; Notch EGF 11-13 domains, grey. The tetra-antennary form of a complex-type N-glycan (dark grey sticks) was modelled onto the JAG1 structure (PDB:4CBZ) based on homologous JAG2 and *Drosophila* Delta structures (PDB:5MWF and 7ALK, respectively) and glycan analysis (see text for details). (**C**) Reducing SDS-PAGE analysis of purified WT JAG1 and the indicated N-glycan variants. Image is representative of $N$=3 independent experiments.

**Fig. 2. JAG1 C2 N-glycan variants show reduced ability to activate Notch in reporter cell lines. (A and B)** Notch receptor activation by JAG1 variants was assessed by mN1-NLuc/CLuc-RBPjk (A) and mN2- NLuc/CLuc-RBPjk (B) reporter cells using a luminescent readout. Data represent combined results of $N$ >4 independent experiments, each with 5 technical repeats. Luminescence signal is presented relative to J1-WT with mean ± SD indicated. Statistical significance was determined by a Kruskal-Wallis test and post-hoc Dunn's multiple comparisons test. Cells-only and Luciferin-only background controls indicated by a black line. (**C**) Median fluorescence intensity **(**MFI) of YFP expression in CHO hN1G4$^{esn}$ reporter cells in response to JAG1 variants. Data represent combined results of $N$=4 independent experiments; 10,000 cells

were measured in each experiment. IgG and cells-only background controls are indicated. Statistical significance was determined by ordinary one-way ANOVA test and Dunnett's post-hoc test. **(D)** One representative experiment of JAG1 variant–mediated Notch activation in CHO hN1G4$^{esn}$ reporter cells showing YFP fluorescence measured by flow cytometry.

**Fig. 3. JAG1 C2 N-glycan variants cause defects in VSMC differentiation.** (**A**) Immunofluorescence microscopy showing the smooth muscle marker α-SMA in VSMCs plated on J1-WT, J1-FL , the N-glycan variant N143A or the Notch binding–deficient negative control F207A/E228K. Scale bar, 100μm. Phalloidin was used to stain actin filaments, and DAPI was used to label nuclei. IgG is a negative control. Images are representative of $N = 3$ independent experiments. (**B**) Western blotting and quantification of α-SMA in VSMCs plated on surfaces coated with the indicated purified JAG1 N-glycan and S142N variants. IgG and JAG1 variants F207A, E228K, and F207A/E228K were used as negative controls. β-tubulin is a loading control. Representative blot is shown, $N = 3$ independent experiments. Quantification of αSMA fold change induced by JAG1 variants and compared to J1-WT. Statistical significance was determined by ordinary one-way ANOVA and Dunnett's post-hoc test (IgG, J1-FL, E228K, N217A excluded).

**Fig. 4. Liposome and Notch binding by N-glycan variants. (A)** J1-WT or mutant variant-coated Protein G beads were incubated with either phosphatidylcholine (PC)- or sphingomyelin (SM)-rich liposomes. Bead population was gated for size, complexity, and fluorescence. SSC, side scatter; FSC, forward scatter. Percentages of beads as aggregates shown for J1-WT and the negative control variant DE3, which lacks the JAG1 C2 domain. **(B)** Quantification of

aggregates formed by ligand-coated beads with PC-rich and SM-rich liposomes. *N*=4 independent experiments. Aggregate percentages are presented as mean ± SD. Background controls (DE3, IgG, and Beads only) are indicated. Statistical analysis was performed using ordinary one-way ANOVA and Dunnett's post hoc test. **(C)** Notch1 binding assay of N-glycan variants. Pre-clustered $NOTCH1_{EGF11\text{-}13}$ was added to wells at high (H, 400 nM) and low (L, 40 nM) concentrations. *N* = 3 independent experiments, each performed in triplicate. Binding is expressed as a percentage of WT signal obtained at the high concentration of NOTCH1. Data presented as mean ± SD. Statistical analysis was performed using Welch's one-way ANOVA and a post hoc Games-Howell test. Each variant was compared to J1-WT. **(D)** Binding to complete Notch1 expressed in HEK293T cells. *N*=3 independent experiments. Data expressed as mean ± SD. Background controls IgG and Cells only are indicated. Statistical analysis was performed by ordinary one-way ANOVA test and a post-hoc Dunnett's test, (J1-FL, F207A, F207A/E228K excluded).

**Fig. 5. Predicted lipid binding modes of the JAG1 C2 domain. (A)** Frequency map showing the protein-to-membrane centre-of-mass distance and the relative protein orientation ($R_{zz}$ is the zz component of the transformation matrix with respect to a reference structure at $R_{zz}$ = 0. $R_{zz}$=-1 is a 180$^o$ rotation). The yellow circle marks the approximative $R_{zz}$ and distance coordinates of a physically possible binding mode. The red circle marks an unphysical binding mode. **(B)** Intermediate, but physically possible, binding mode of C2 (yellow, from PDB 4CBZ), bound to a PC:PS (75:25) lipid membrane (PC and PS heads in black and red, respectively). Only C2 was simulated, but other parts of the complex have been superimposed onto the C2 binding mode: glycan on *Drosophila* Delta from PBD 7ALK (cyan), rat Jag1 DSL EGF1-3 from PDB 5UK5

(orange), rat Notch1 EGF8-12 from PBD 5UK5 (green), and rat Notch1 EGF13 from PDB 4XL1 (purple). **(C)** Unphysical binding mode with steric clashes, same structures superimposed.

A

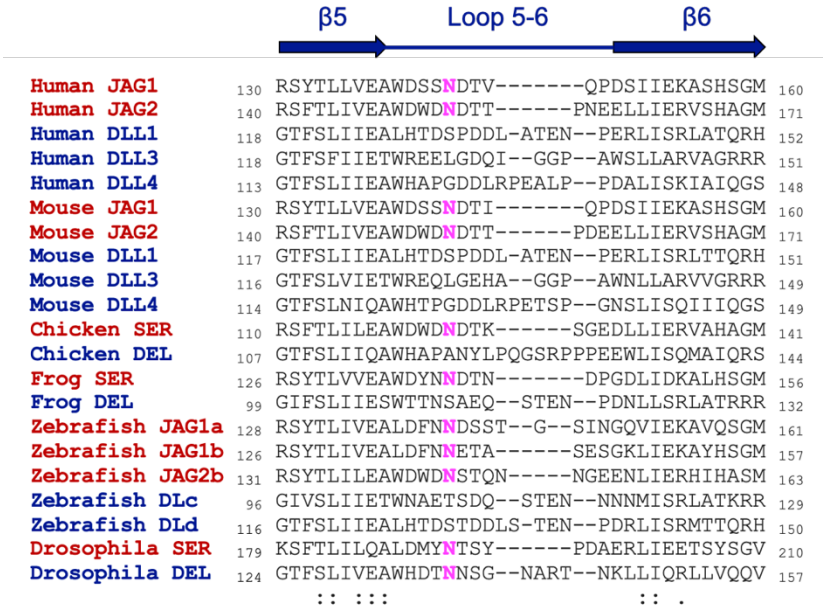
β5
Loop 5-6
β6
Human JAG1 130 RSYTLLVEAWDSSNDTV-------QPDSIIEKASHSGM 160
Human JAG2 140 RSFTLIVEAWDWDNDTT------PNEELLIERVSHAGM 171
Human DLL1 118 GTFSLIIEALHTDSPDDL-ATEN--PERLISRLATQRH 152
Human DLL3 118 GTFSFIIETWREELGDQI--GGP--AWSLLARVAGRRR 151
Human DLL4 113 GTFSLIIEAWHAPGDDLRPEALP--PDALISKIAIQGS 148
Mouse JAG1 130 RSYTLLVEAWDSSNDTI-------QPDSIIEKASHSGM 160
Mouse JAG2 140 RSFTLIVEAWDWDNDTT------PDEELLIERVSHAGM 171
Mouse DLL1 117 GTFSLIIEALHTDSPDDL-ATEN--PERLISRLTTQRH 151
Mouse DLL3 116 GTFSLVIETWREQLGEHA--GGP--AWNLLARVVGRRR 149
Mouse DLL4 114 GTFSLNIQAWHTPGDDLRPETSP--GNSLISQIIIQGS 149
Chicken SER 110 RSFTLILEAWDWDNDTK------SGEDLLIERVAHAGM 141
Chicken DEL 107 GTFSLIIQAWHAPANYLPQGSRPPPEEWLISQMAIQRS 144
Frog SER 126 RSYTLVVEAWDYNNDTN-------DPGDLIDKALHSGM 156
Frog DEL 99 GIFSLIIESWTTNSAEQ--STEN--PDNLLSRLATRRR 132
Zebrafish JAG1a 128 RSYTLIVEALDFNNDSST--G--SINGQVIEKAVQSGM 161
Zebrafish JAG1b 126 RSYTLIVEALDFNNETA------SESGKLIEKAYHSGM 157
Zebrafish JAG2b 131 RSYTLILEAWDWDNSTQN-----NGEENLIERHIHASM 163
Zebrafish DLc 96 GIVSLIIETWNAETSDQ--STEN--NNNMISRLATKRR 129
Zebrafish DLd 116 GTFSLIIEALHTDSTDDLS-TEN--PDRLISRMTTQRH 150
Drosophila SER 179 KSFTLILQALDMYNTSY------PDAERLIEETSYSGV 210
Drosophila DEL 124 GTFSLIVEAWHDTNNSG--NART--NKLLIQRLLVQQV 157

B

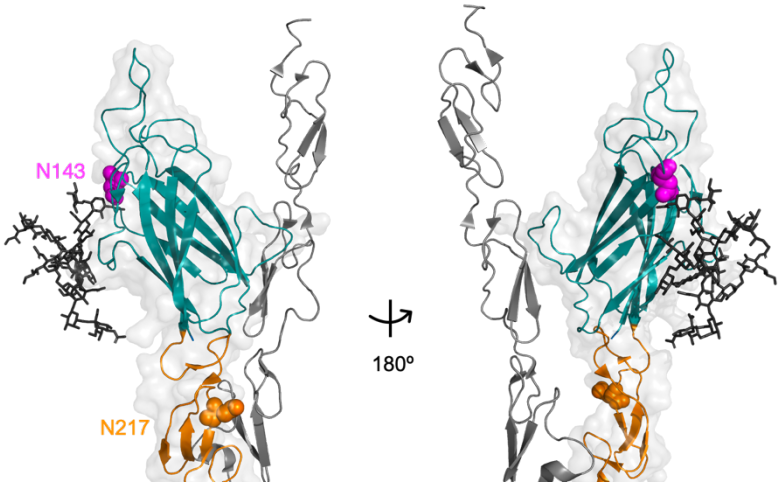
N143
N217
180°

C

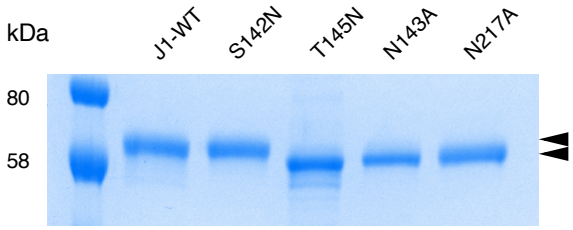
kDa
J1-WT
S142N
T145N
N143A
N217A
80
58

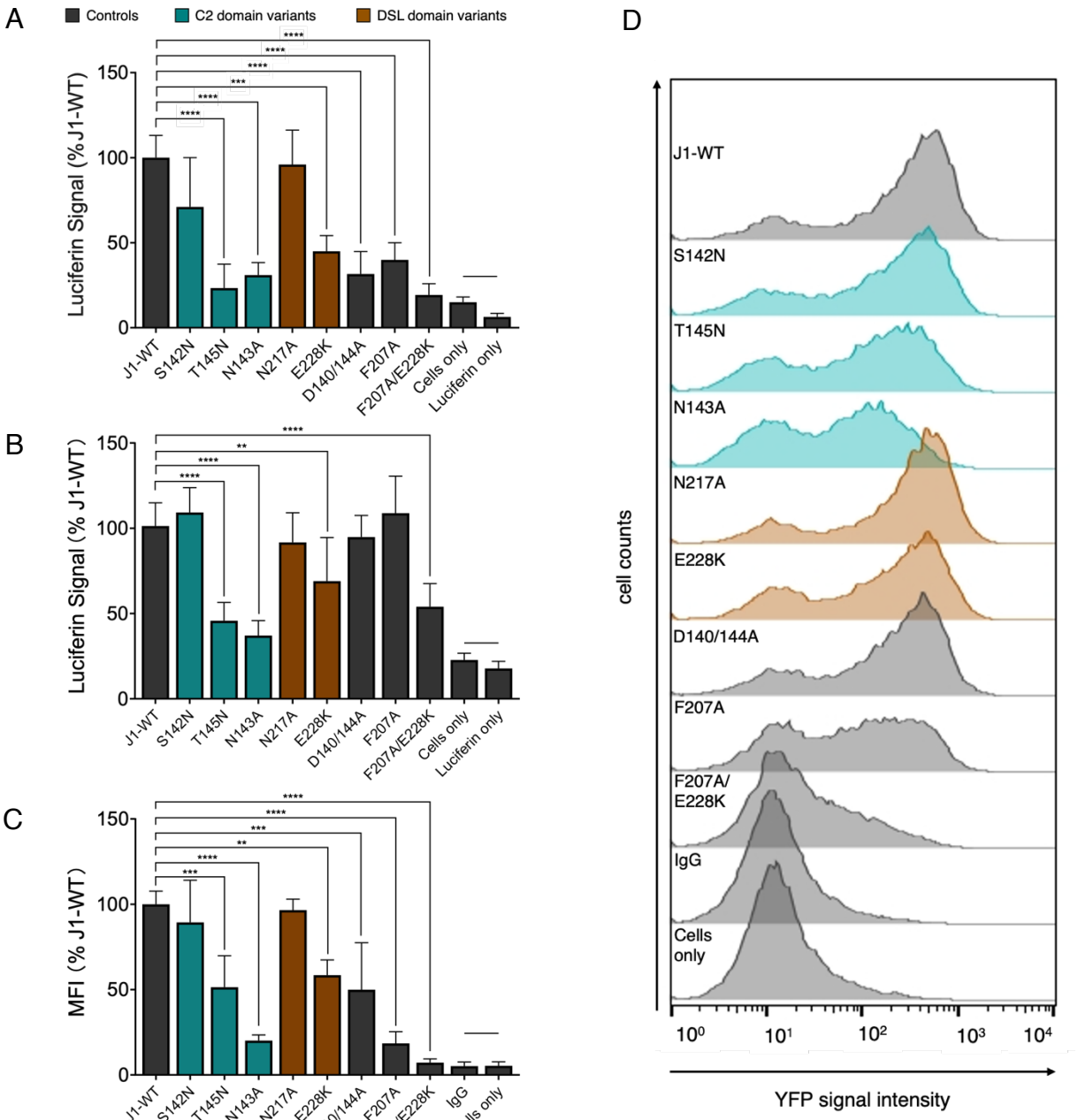
A
Controls
C2 domain variants
DSL domain variants
Luciferin Signal (%J1-WT)
150
100
50
0
J1-WT
S142N
T145N
N143A
N217A
E228K
D140/144A
F207A
F207A/E228K
Cells only
Luciferin only
B
Luciferin Signal (% J1-WT)
Luciferin only
C
MFI (% J1-WT)
IgG
D
cell counts
J1-WT
S142N
T145N
N143A
N217A
E228K
D140/144A
F207A
F207A/
E228K
IgG
Cells
only
$10^0$
$10^1$
$10^2$
$10^3$
$10^4$
YFP signal intensity

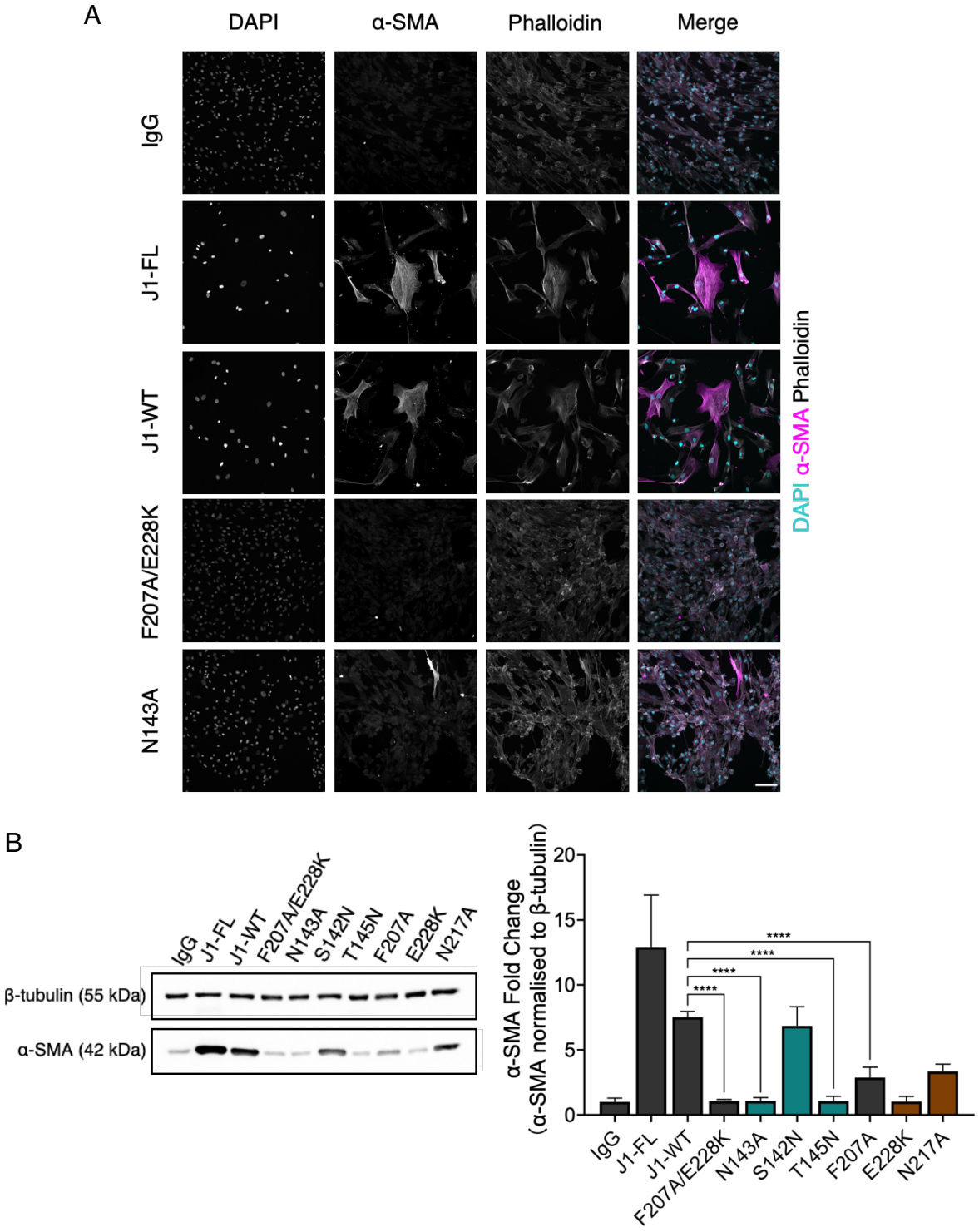
A
DAPI
α-SMA
Phalloidin
Merge
IgG
J1-FL
J1-WT
F207A/E228K
N143A
DAPI α-SMA Phalloidin
B
IgG
J1-FL
J1-WT
F207A/E228K
N143A
S142N
T145N
F207A
E228K
N217A
β-tubulin (55 kDa)
α-SMA (42 kDa)
α-SMA Fold Change
(α-SMA normalised to β-tubulin)
20
15
10
5
0
****
****
****
****
IgG
J1-FL
J1-WT
F207A/E228K
N143A
S142N
T145N
F207A
E228K
N217A

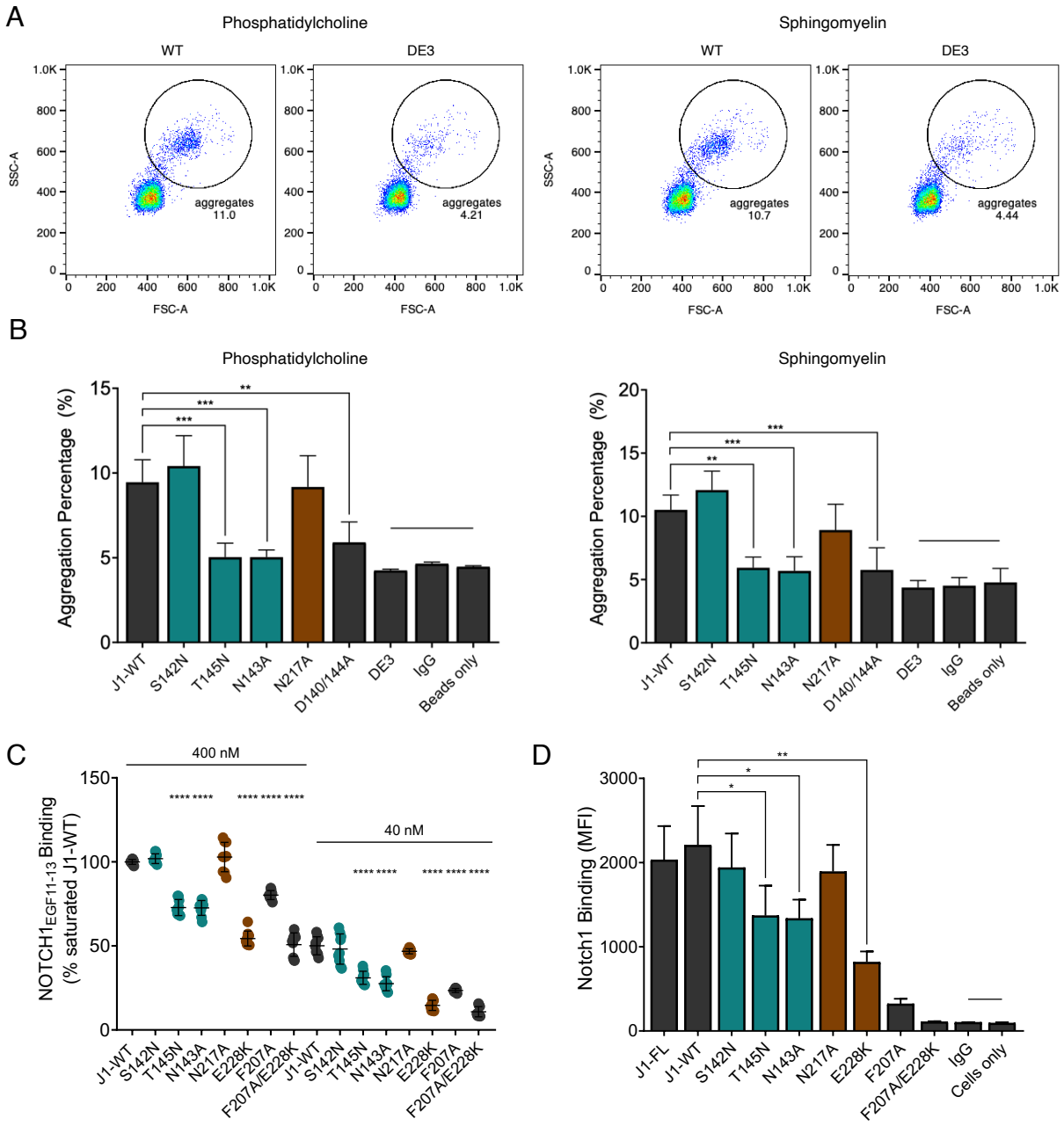
A
Phosphatidylcholine
Sphingomyelin
WT
DE3
SSC-A
FSC-A
aggregates
11.0
4.21
10.7
4.44
B
Aggregation Percentage (%)
J1-WT
S142N
T145N
N143A
N217A
D140/144A
DE3
IgG
Beads only
C
400 nM
40 nM
NOTCH1EGF11-13 Binding
(% saturated J1-WT)
E228K
F207A
F207A/E228K
D
Notch1 Binding (MFI)
J1-FL
Cells only

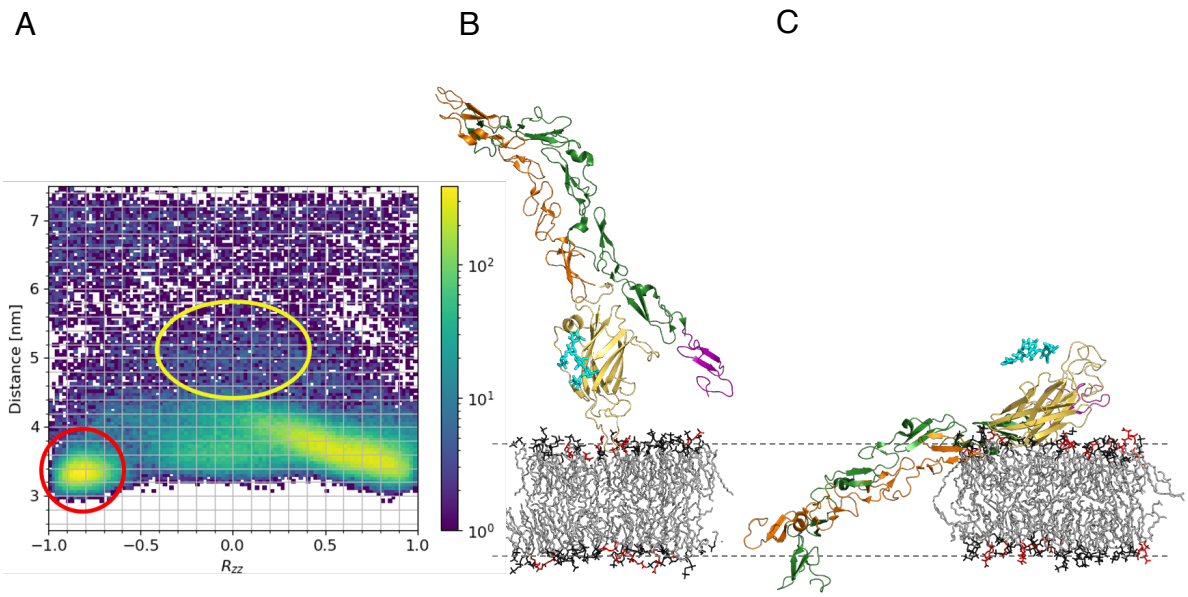
A
B
C
Distance [nm]
7
6
5
4
3
−1.0
−0.5
0.0
0.5
1.0
$R_{zz}$
$10^2$
$10^1$
$10^0$

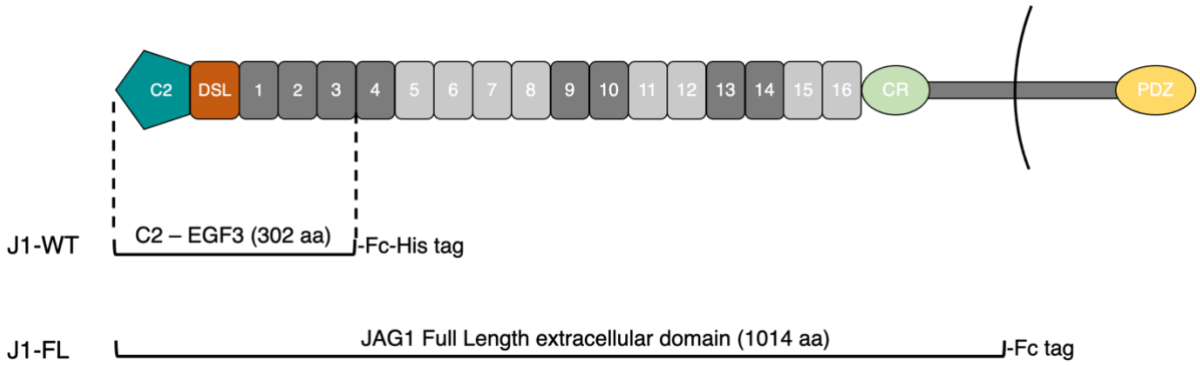


**Fig. S1. Domain organization of JAG1 constructs J1-WT and J1-FL used in this study.** Complete domain organization of JAG1 shown with C2, DSL, EGF domains 1-16 (numbered) Cysteine-rich region (CR) and PDZ intracellular domain. The N-terminal fragment J1-WT was expressed in HEK cells as a soluble Fc tag fusion protein which was purified in its dimerized form. COSMIC and protein engineered variants of the C2 domain were constructed using J1-WT cDNA as starting template. J1-FL with an Fc-tag was obtained commercially as described in Materials and methods.

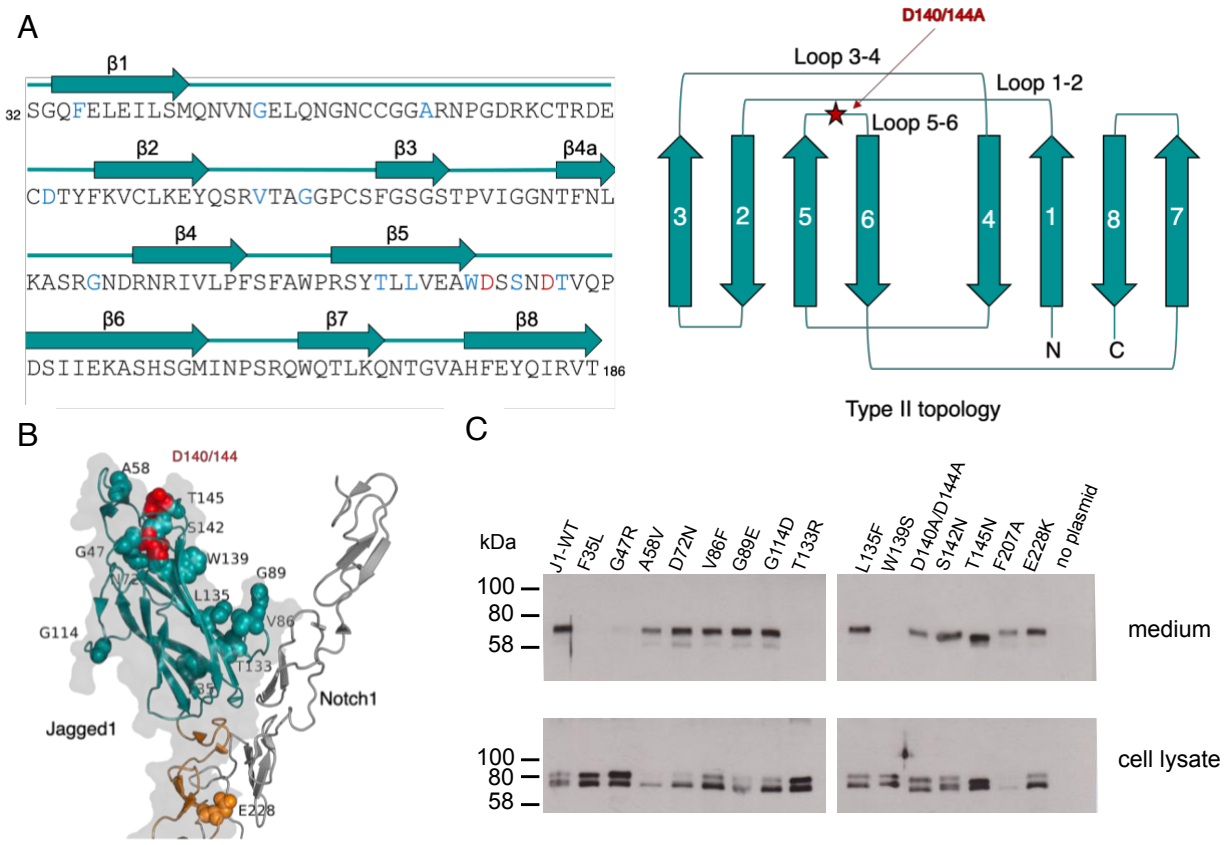


**Fig. S2. Effects of JAG1 COSMIC variants on secretion and activation. (A)** Primary sequence and type II topology of JAG1 C2 domain shown with positions of COSMIC substitutions shown in blue, together with D140-D144 residues which contribute to the C2 apical calcium-binding site. **(B)** Substitutions associated with COSMIC variants, together with D140/D144 indicated on Jagged1/Notch complex structure (PDB: 5UK5, 2VJ3) C2 shown in teal, DSL in orange, Notch in grey. **(C)** Western blot of expression of COSMIC variants compared to J1-WT. Equivalent volumes of medium and cell lysate samples were collected and separated by 10% reducing SDS-PAGE. The molecular weight (MW) of monomeric J1-WT is 61 kDa but it migrated at a higher MW due to glycosylation. A subset of COSMIC variants were expressed but cause protein misfolding and are retained in the cell (F35L, G47R, T133R, W139S). Others are secreted similarly to J1-WT. A polyclonal anti-His-HRP rat antibody was used for signal detection. Three independent transfections were performed, and a representative western blot is shown. Molecular weight markers (kDa) are indicated.

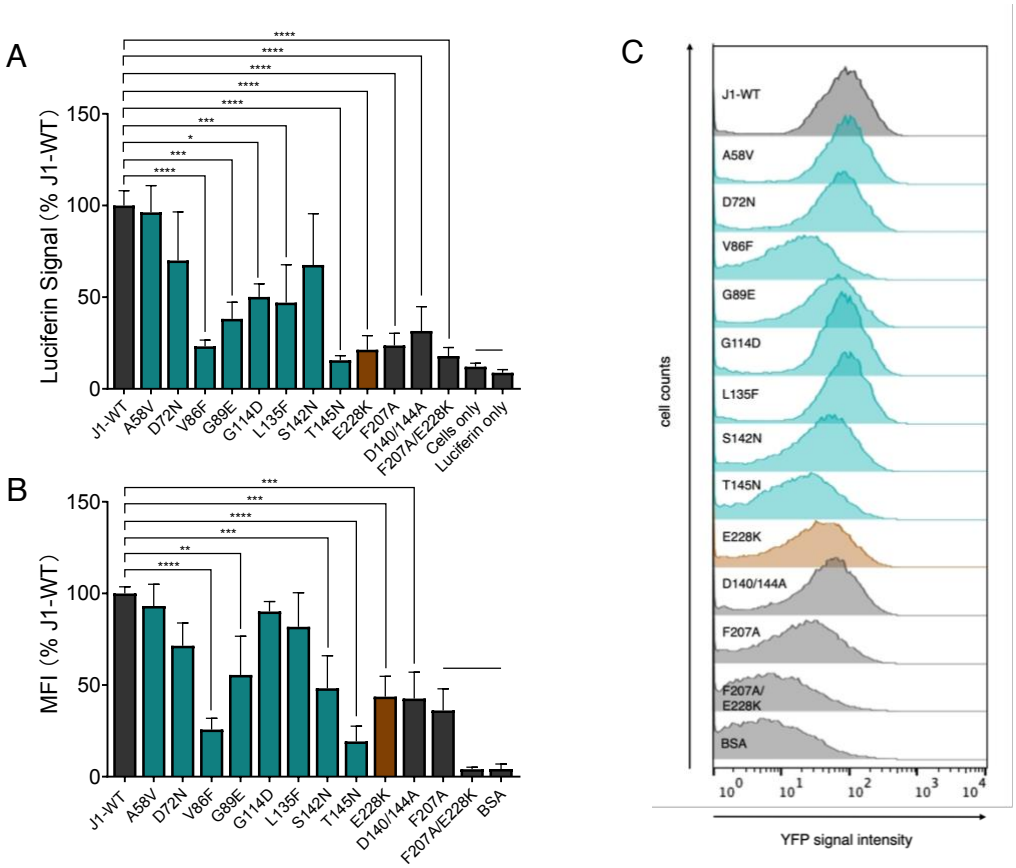


D

| Domain | Missense mutation | Position at C2 domain | Secretion | Luciferase Notch1 activation | CHO-YFP Notch1 activation |
|---|---|---|---|---|---|
| C2 | F35L | beta sheet 1 | X | n/a | n/a |
| C2 | G47R | loop1-2 | X | n/a | n/a |
| C2 | A58V | loop1-2 | ✓ | no effect | no effect |
| C2 | D72N | loop1-2 | ✓ | no effect* | no effect* |
| C2 | V86F | loop2-3 | ✓ | low[1] | low[2] |
| C2 | G89E | loop2-3 | ✓ | intermediate[1] | intermediate[2] |
| C2 | G114D | loop3-4 | ✓ | intermediate[1] | no effect |
| C2 | T133R | beta sheet 5 | X | n/a | n/a |
| C2 | L135F | beta sheet 5 | ✓ | intermediate[1] | no effect |
| C2 | S142N | loop5-6 | ✓ | no effect | intermediate[2] |
| C2 | T145N | loop5-6 | ✓ | low[1] | low[2] |
| C2 | W139S | beta sheet 5 | X | n/a | n/a |
| DSL | E228K | n/a | ✓ | low[1] | low[2] |

**Fig. S3. Notch activation assays using purified COSMIC variants. (A)** Split luciferase Notch activation assay of JAG1 COSMIC variants by mN1-NLuc/CLuc-RBPjk reporter cells. Data combined from three independent experiments (each with 5 technical replicates). The average value of activation by J1-WT was taken to be 100%. Results were expressed as a percentage of J1-WT activation. Data presented as mean ± SD. Cells only and Luciferin only were background controls. Comparisons between groups were performed with the Kruskal Wallis test followed by a post-hoc Dunn's test. JAG1 protein controls are in dark grey, COSMIC variants in C2 (teal) in DSL (brown). **(B)** MFI quantification of Notch activation assay using CHO hN1G4$^{esn}$ cells. The average MFI value of activation by J1-WT was taken to be 100%. Three independent experiments were performed, and data from 6,000 single cells were recorded for each variant. Data presented as mean ± SD Statistical analysis was performed using an ordinary one-way ANOVA followed by Dunnett's post-hoc test (F207A, F207A/E228K, BSA data sets were excluded). **(C)** Representative flow cytometry histogram of COSMIC variants (C2-teal, DSL-brown) with J1-WT and negative controls (grey). **(D)** Summary of COSMIC variant effects on secretion and activation. COSMIC variants showed high, intermediate and low levels of activity, although the intermediate group were not all statistically significantly different in both assays. "Intermediate" variant was defined as having an activity (% J1-WT)[1] or a peak maximum[2] which occurs at greater or similar fluorescence intensity compared to D140/144A, but lower than the WT. A "low" variant has activity (% J1-WT)[1] or a peak maximum[2] which occurs at a lower fluorescence intensity than D140/144A. Note that S142N showed a similar distribution as D140/144A in individual repeat experiments and is classed as "intermediate". * D72N was not statistically significant in reporter assays, but showed a lower mean value than J1-WT in each case.

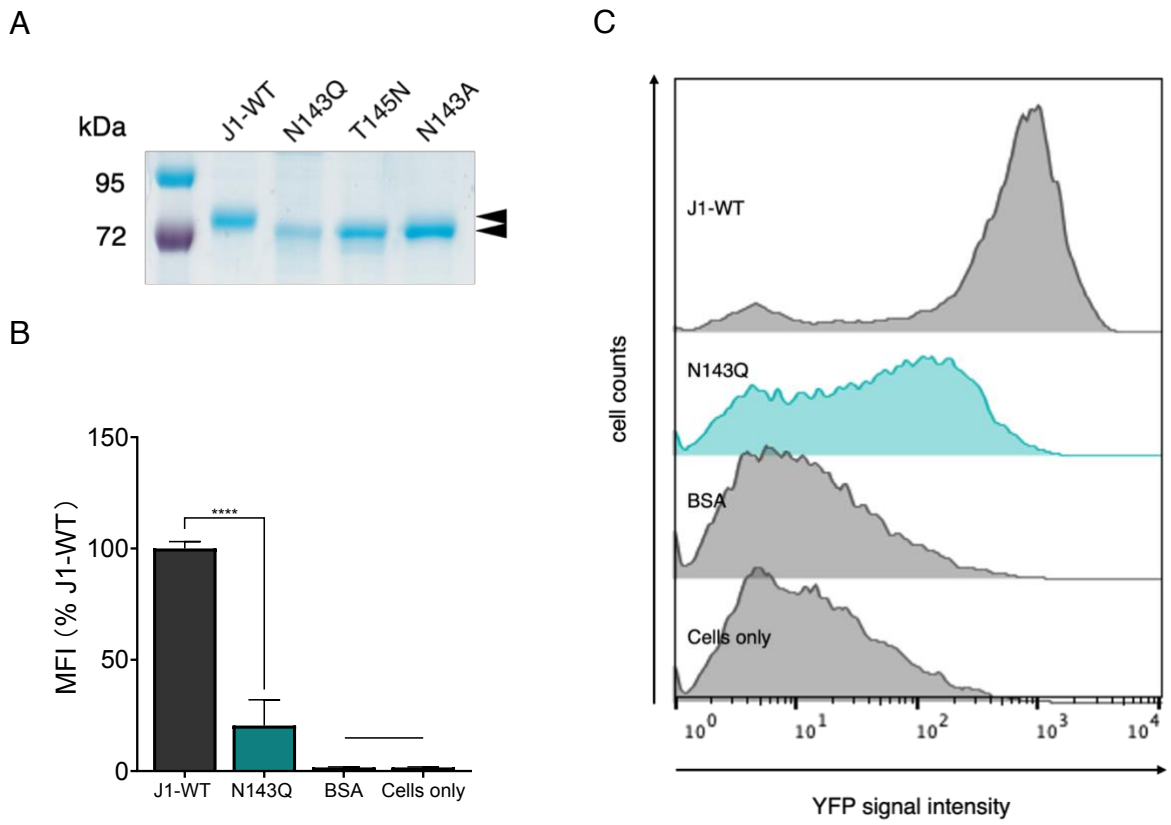


**Fig. S4. Notch activation by N143Q using CHO hN1G4$^{esn}$ cells. (A)** Purified N143Q was analysed by reducing 10% SDS-PAGE together with J1-WT, N143A and T145N. Like T145N and N143A, purified N143Q showed a MW drop compared to J1-WT (indicated by black arrowheads). Image representative of 3 independent experiments. **(B)** MFI quantification of CHO-YFP activation assay. 3 independent experiments were performed, and MFI values presented relative to J1-WT. Data presented as mean ± SD. BSA and Cells only were negative controls. Statistical analysis was performed using the Mann-Whitney test. **(C)** A representative flow cytometry histogram of CHO-YFP fluorescence is shown.

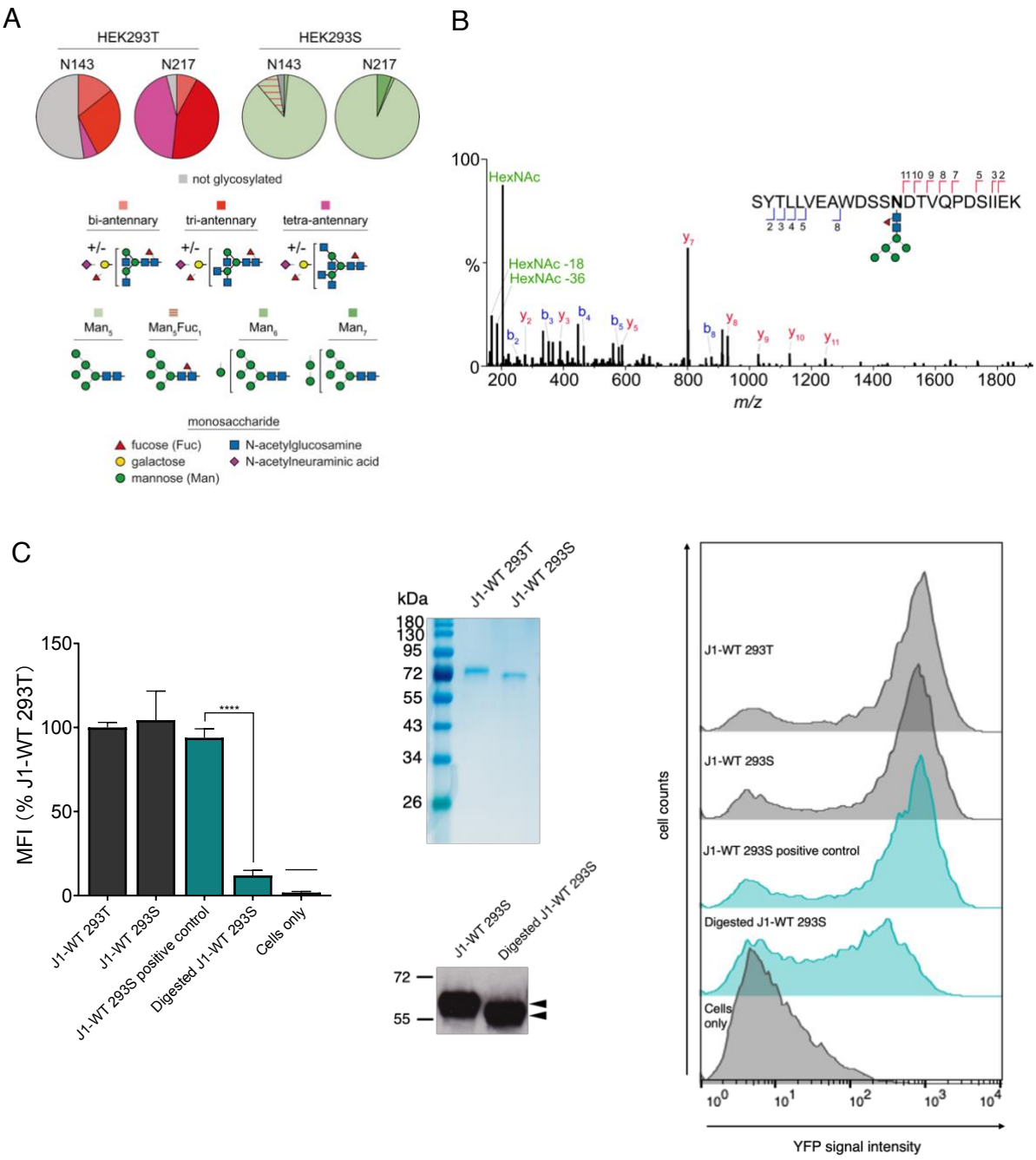
A
HEK293T
HEK293S
N143
N217
N143
N217
not glycosylated
bi-antennary
tri-antennary
tetra-antennary
+/-
+/-
+/-
Man5
Man5Fuc1
Man6
Man7
monosaccharide
fucose (Fuc)
galactose
mannose (Man)
N-acetylglucosamine
N-acetylneuraminic acid
B
100
%
0
HexNAc
HexNAc -18
HexNAc -36
SYTLLVEAWDSSNDTVQPDSIIEK
200
400
600
800
1000
1200
1400
1600
1800
m/z
C
MFI (% J1-WT 293T)
150
100
50
0
****
J1-WT 293T
J1-WT 293S
J1-WT 293S positive control
Digested J1-WT 293S
Cells only
kDa
J1-WT 293T
J1-WT 293S
180
130
95
72
55
43
34
26
J1-WT 293S
Digested J1-WT 293S
72
55
cell counts
J1-WT 293T
J1-WT 293S
J1-WT 293S positive control
Digested J1-WT 293S
Cells only
YFP signal intensity

**Fig. S5. Glycoproteomic analysis of J1-WT purified from HEK293T and HEK293S cells.** Complex-type (produced from HEK293T) and high mannose (produced from HEK293S) N-glycans with different branches were observed by mass spectrometry analysis. The Asn-linked GlcNAc was modified by fucose at both N143 (C2 domain) and N217 (DSL) sites. **(A)** Pie graphs show composition of N-glycans on tryptic peptides produced from HEK293S and HEK293T cells covering two different sites of J1-WT construct analysed. Site 1 indicates Asn143, and site 2 indicates Asn217. **(B)** Tandem MS/MS spectrum of the N143 glycopeptide showing the presence of a $Man_5Fuc_1$ glycan. Oxonium ions are labelled green plus b- and y- ion series. **(C)** Notch activation of J1-WT purified from 293S cells were assessed using CHO hN1G4$^{esn}$ cells. MFI of J1-WT 293S ( PNGase F- cleaved and undigested) and J1-WT 293T samples. $n \geq 3$ independent experiments. Data presented as mean ± SD, Statistical analysis was performed using the Kruskal-Wallis test and Dunn's post-hoc test. Reducing 10% SDS-PAGE analysis showing purified J1 from HEK293S and HEK293T. Western blot showing MW drop (indicated by black arrows) after digestion of 293S J1-WT by PNGase F. Representative YFP histograms of CHO N1 activation by 293S (PNGase F digested and undigested) and 293T samples of J1-WT.

A

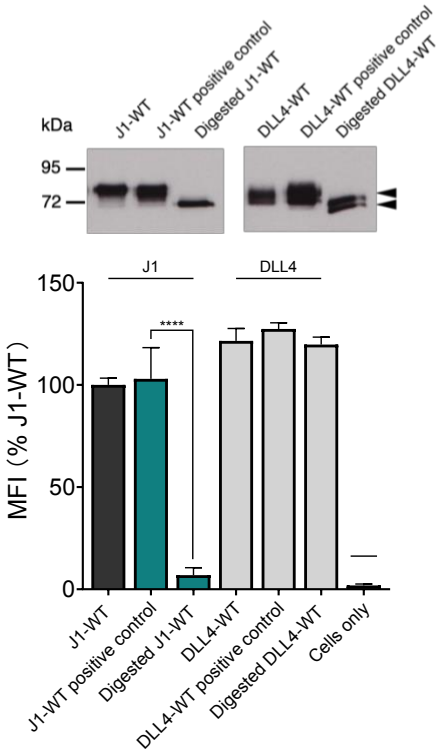
kDa
J1-WT
J1-WT positive control
Digested J1-WT
DLL4-WT
DLL4-WT positive control
Digested DLL4-WT
95
72
J1
DLL4
MFI (% J1-WT)
150
100
50
0
****
J1-WT
J1-WT positive control
Digested J1-WT
DLL4-WT
DLL4-WT positive control
Digested DLL4-WT
Cells only

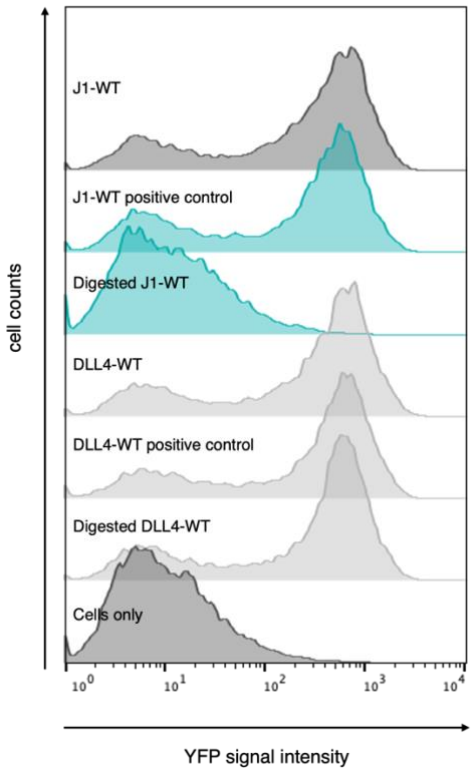
cell counts
J1-WT
J1-WT positive control
Digested J1-WT
DLL4-WT
DLL4-WT positive control
Digested DLL4-WT
Cells only
$10^0$
$10^1$
$10^2$
$10^3$
$10^4$
YFP signal intensity

B

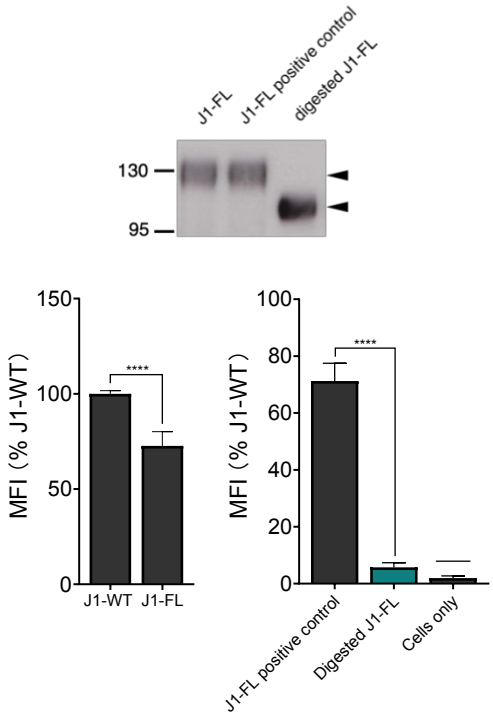
J1-FL
J1-FL positive control
digested J1-FL
130
95
MFI (% J1-WT)
150
100
50
0
****
J1-WT
J1-FL
MFI (% J1-WT)
100
80
60
40
20
0
****
J1-FL positive control
Digested J1-FL
Cells only

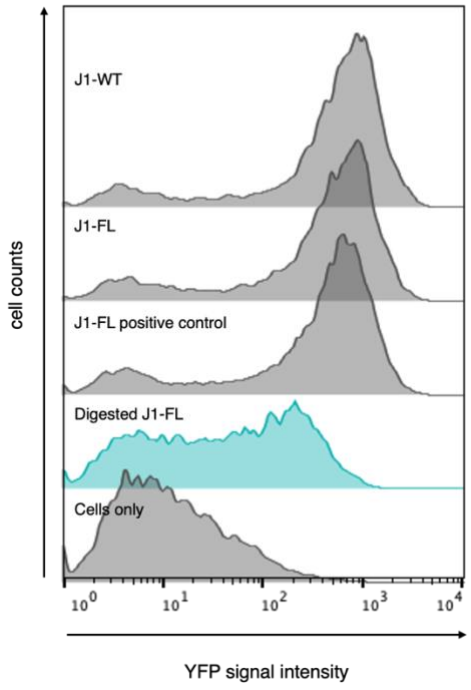
cell counts
J1-WT
J1-FL
J1-FL positive control
Digested J1-FL
Cells only
$10^0$
$10^1$
$10^2$
$10^3$
$10^4$
YFP signal intensity

**Fig. S6. Notch activation assay using J1-WT and the full-length extracellular domain of Jagged1 (J1-FL).** **(A)** J1-WT purified from HEK293T cells, PNGase F digested samples (Digested J1-WT) and the positive control incubated under similar conditions (J1-WT positive control) were viewed by western blot together with equivalent DLL4 samples (comprising C2, DSL and EGF1-3 domains) which lack the C2 N-glycan. A lower molecular weight band (indicated by black arrowhead) was observed in the PNGase F digested samples only. CHO hN1G4$^{esn}$ Notch1 activation assay of PNGaseF-digested forms, (Cells only-negative control). Data from 10,000 single cells from each sample were recorded. MFI of YFP signal was normalised to J1-WT. *N*=3 independent experiments, data were combined for quantification and presented as mean ± SD. Comparison of J1-WT and DLL4-WT sample groups (light grey) was assessed using Kruskal-Wallis test followed by Dunn's post-hoc test. A representative histogram is shown. **(B)** Normal and digested forms of J1-FL purified protein were assessed for activity using CHO hN1G4$^{esn}$ cells. Digested J1-FL showed a MW drop compared to controls. MFI of YFP signal from CHO hN1G4$^{esn}$ cells shown, *N*=3 independent experiments, data presented as mean ± SD. Statistical analysis was performed using the Kruskal-Wallis test followed by Dunn's multiple comparisons test. A representative histogram is presented.

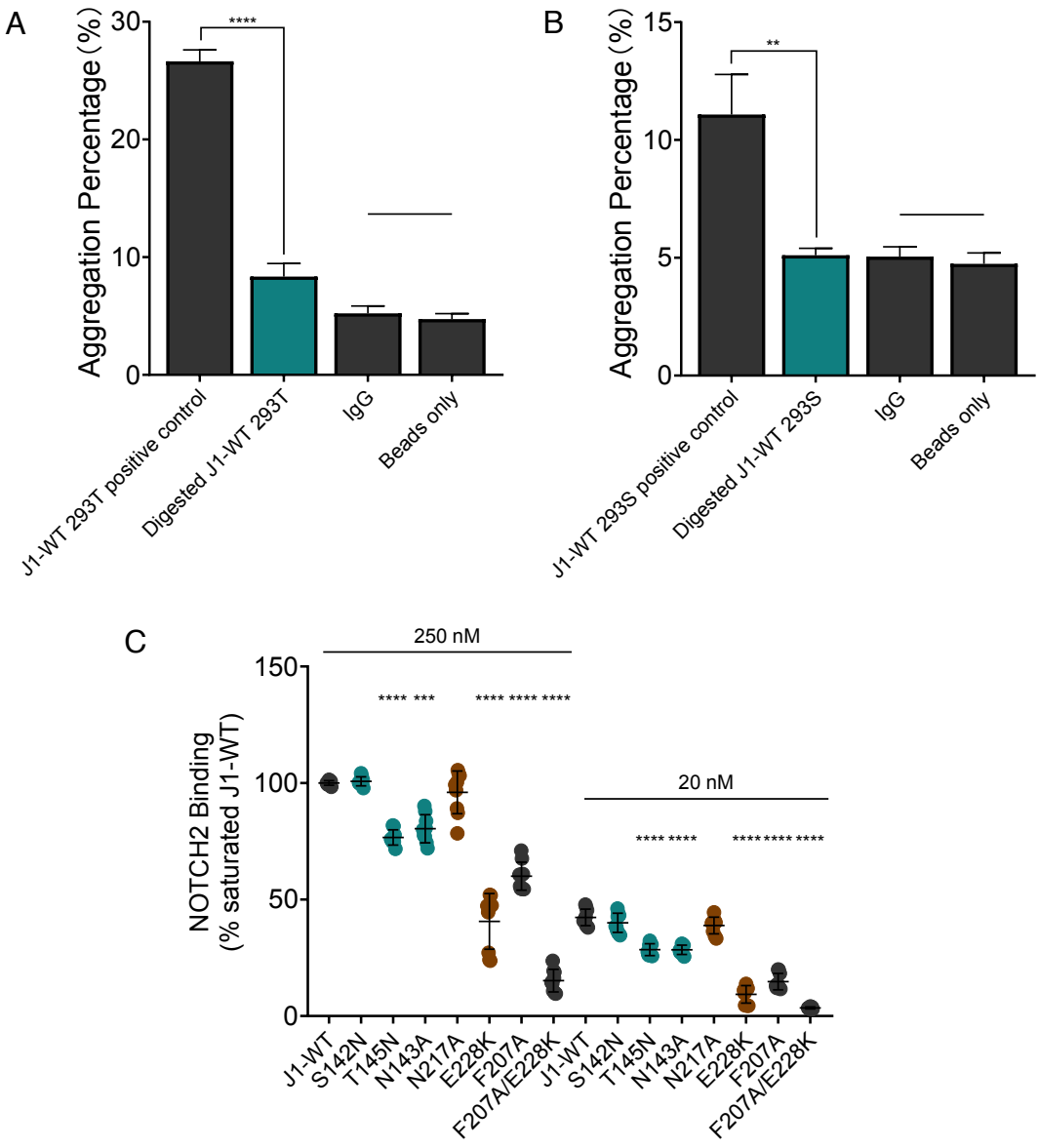


**Fig. S7. Liposome binding of PNGase F digested WT-J1 and NOTCH2 binding of C2 N-glycan variants.** **(A and B)** Liposome binding of PNGase F-digested J1-WT samples purified from HEK293T (A) and HEK293S cells (B) were tested using PC-rich liposomes. Background controls were IgG and beads only, 3 independent experiments were performed, and combined data presented as mean ± SD. Data were analysed using an unpaired t-test in each case. **(C)** NOTCH2 binding assay of N-glycan variants using NOTCH2 EGF11-13 purified fragments. *N*=3 independent experiments, each performed in triplicate. Binding was expressed as a percentage of J1-WT signal obtained at the high concentration of NOTCH2. Data presented as mean ± SD. Statistical analysis was performed using a Welch one-way ANOVA test and a Games-Howell post-hoc test.